Chapter 2
Modeling Cellular Dynamics

Cells are the basic units of biological structure and functions. They make up tissues and our bodies. A single cell includes organelles and intracellular solutions, and it is separated from outer environment of extracellular liquid surrounding the cell by its cell membrane (plasma membrane), generating differences in concentrations of ions and molecules including enzymes. The differences in charges of ions and concentrations cause, respectively, electrical and chemical potentials, generating transportations of materials across the membrane. Here we look at cores of mathematical modeling associated with dynamic behaviors of single cells as well as bases of numerical simulations.

2.1 Ion Channels and Cellular Excitations

The difference in the intra and extra-cellular electrical potential is referred to as the *membrane potential*. The cellular membrane potential shows dynamic changes either spontaneously or in response to external stimulations that are electrical, chemical, and/or mechanical.

Figure 2.1 exemplifies such changes in the membrane potential in neuronal cells of a cat spinal cord, in which the membrane potential shows a single spiky change on the left (A) and repetitive burst-like changes on the right (B). Each of the spiky transient increase and decrease is referred to as the *action potential*, or in cases of neuronal cells, the *spike*. In Fig. 2.1 (B), in particular for the set of two traces at the middle, we can observe two different phases alternate almost periodically. In one phase, spikes are generated with high frequency (active phase of the burst), and no spikes in the other phase (silent phase of the burst). Action potentials play significantly important roles for functions of cells, and thus for functions of cellular tissues and organs. The neuronal cells used in the experiment for Fig. 2.1 are associated with the control of muscle contractions actuating motions of the animal's limbs during rhythmic walking. This means that the sequences of action potentials of the neuronal cells "encode" and transmit information on the muscular force intensities and timings, i.e., how much the muscles that are controlled somehow by those cells would generate the force and how the force would change along the time.

T. Nomura and Y. Asai, *Harnessing Biological Complexity*, A First Course in "In Silico Medicine" 1, DOI 10.1007/978-4-431-53880-6_2, © Springer 2011

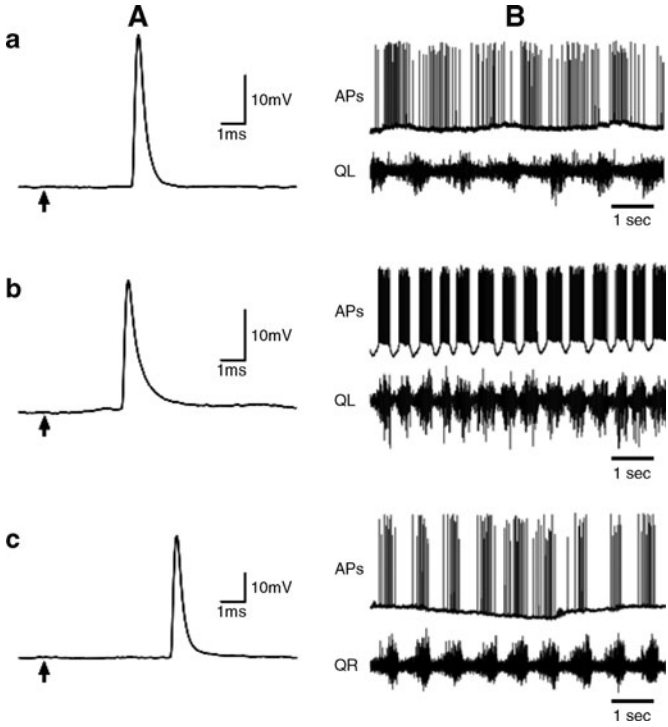


Fig. 2.1 (**A**) Action potentials of spinal commissural interneurons (**a, b**) and a spinal neuron with a long ascending axon (**c**), all of which were recorded intraaxonally in the lumbar spinal cord of decerebrate, immobilized cats. The potentials in **a** and **b** were evoked monosynaptically by stimulation to the medullary reticular formation. The potential in **c** were evoked antidromically by stimulation to the same reticular area, thus indicating that the neuron extend its axon rostrally up to the reticular formation in the brainstem. Upward arrows in **a–c** indicate timings of the stimulation. (**B**) Locomotion-related discharge activities of three spinal neurons **a–c** during the generation of fictive locomotion, which was evoked by stimulation to the mesencephalic locomotor region. In each figure, the upper trace represents rhythmic discharges of neuronal action potentials (APs), and the lower trace shows activities of electroneurograms recorded from the left or right quadriceps nerves (QL or QR). This figure is made available here through the courtesy of Prof. Kiyoji Matsuyama

Indeed, this can be better understood by looking at the lower trace of each of three recordings (upper, middle, and lower) of Fig. 2.1B, which is the electroneurogram recorded from the left or right quadriceps nerves, representing the total neural command delivered to the muscle to induce muscle contractions. In the middle and lower traces of Fig. 2.1B, the active phases of the burst correspond to the large activities of the electroneurogram, implying that the neural system commands the muscle to perform large contractions.

Muscle cells such as cardiac heart cells and skeletal muscles also generate action potentials that control contractions of the muscle fibres as we will see later in this chapter. Pancreatic β cells show burst-like action potentials in response to an increase in glucose concentration in the blood in order to control the amount of insulin gene expression and secretion as we will also see briefly in this chapter.

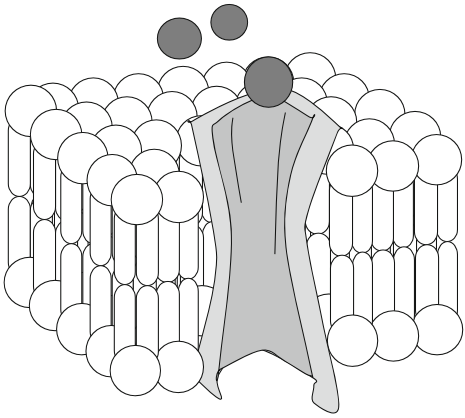


Fig. 2.2 Schematic illustration of cross-section of a single ion channel protein that forms a pore and is embedded in the lipid-bilayer of the cellular membrane

Action potentials and many other dynamic activities of a cell are induced and/or modulated by communications between the cell and its environment. Such communications are achieved through membrane channels and receptors. Figure 2.2 schematically illustrates an ion channel protein which is embedded in the membrane to allow flows of ions across the membrane. Such a protein forms a pore and controls influx and efflux of several kinds of ions. The flow of ions can generate dynamic changes in the membrane potential which plays important roles for intra-cellular signal transmission such as calcium signaling as well as inter-cellular communications at tissue level.

2.1.1 A Simple Open–Close Kinetics of a Channel Protein

A typical ion channel allows influx and efflux of a specific type of ions. This property is referred to as the *ion selectivity*. For example, a single potassium channel protein forms a pore which is selective to potassium ions K^+. Ion channels are not merely passive pores, but they actively controls the flow of ions by opening and closing the channels. Let us consider a large number of a specific type of channels embedded in a membrane of a single cell. Let N be the total number of the channels. They allow the flow of a specific type of ions. We assume, as the simplest case, that each of the channels takes one of two states, namely "closed" and "open." See Fig. 2.3. The open state allows the ions to flow through the channel, but the closed state does not. Let $p(t)$ be a fraction of the open state over all the channels at a time instant t, i.e.,

$$p(t) = \frac{\#\text{ of the channels at the open state}}{N}$$

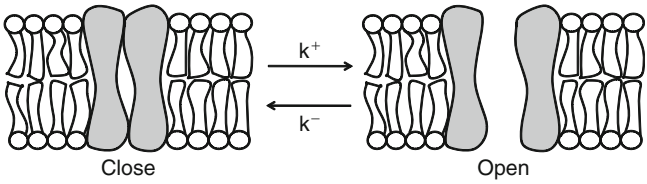


Fig. 2.3 A simple open–close kinetics for a single ionic channel with the rate constants k^- and k^+

Then the fraction of the closed state $q(t)$ can be expressed as

$$\begin{aligned} q(t) &= \frac{\#\text{ of the channels at the close state}}{N} \\ &= \frac{N - \#\text{ of the channels at the open state}}{N} \\ &= 1 - p(t) \end{aligned}$$

Let us consider a single channel among $Np(t)$ at the open state at time t. The channel makes a transition from the open to the closed state stochastically. If the transition is governed by a Poisson point process with its rate or intensity k^-, the probability that a single transition occurs for an infinitesimal small time interval Δt is $k^-\Delta t$. Indeed, this is a definition of the Poisson point process. Moreover if every channel at the open state makes such a transition independently, the mean (ensemble averaged through all the channels) number of the transitions from the open to the closed state within Δt would be $Np(t) \cdot k^-\Delta t$. The number k^- is referred to as the *rate constant*. The reverse transitions can be described similarly by considering the probability that a single transition from the closed state to the open state occurs for an infinitesimal small time interval Δt is $k^+\Delta t$. Thus, the mean number of channels at the open state at time $t + \Delta t$ can be described as follows:

$$Np(t + \Delta t) = Np(t) - Np(t) \cdot k^-\Delta t + N\,(1 - p(t)) \cdot k^+\Delta t$$

which is reformulated as

$$\frac{p(t + \Delta t) - p(t)}{\Delta t} = -k^- p(t) + k^+\,(1 - p(t))$$

It becomes an ordinary differential equation (ODE) as $\Delta t \to 0$, i.e.,

$$\begin{aligned} \frac{dp(t)}{dt} &= -k^- p(t) + k^+\,(1 - p(t)) \\ &= -(k^- + k^+)\left(p(t) - \frac{k^+}{k^- + k^+}\right). \end{aligned} \tag{2.1}$$

Defining $\tau = 1/(k^- + k^+)$ and $p_\infty = k^+/(k^- + k^+)$, we have

$$\frac{dp}{dt} = -\frac{p - p_\infty}{\tau} \tag{2.2}$$

A solution of (2.2) can be obtained analytically by integrating (2.2). This can be done as follows. First, put $x(t) = p(t) - p_\infty$ for the ease of our calculation. Then $dx(t)/dt = dp(t)/dt$, i.e., $dx = dp$, since p_∞ is constant, leading to a new ODE for x as

$$\frac{dx}{dt} = -\frac{x}{\tau}$$

with $x(0) = p(0) - p_\infty$, the initial condition, where $p(0)$ is the open fraction of the channel at the initial time $t = 0$. This can be further rewritten as

$$\frac{dx}{x} = -\frac{1}{\tau}dt.$$

Integrating both sides by x and u (representing time here instead of t), we have

$$\int_{x(0)}^{x(t)} \frac{dx}{x} = -\int_0^t \frac{1}{\tau}du, \tag{2.3}$$

obtaining the solution of (2.2) in terms of $p(t)$ as

$$p(t) = p(0)\exp\left(-\frac{t}{\tau}\right) + p_\infty\left(1 - \exp\left(-\frac{t}{\tau}\right)\right) \tag{2.4}$$

Note that the dynamic variable $p(t)$ of the ODE represents either the open fraction of the channel at time t if we consider all N channels on the membrane or the open probability if we consider a single channel among N channels.

Exercise 2.1. Derive (2.2) from (2.1). Perform the integration in (2.3) to find $x(t)$. Then transform $x(t)$ back to $p(t)$ to obtain the solution as in (2.4).

IDE Modeling: A Simple Channel Kinetics: Search ModelDB by "Kinetics" to Find Simple_Channel_Model.isml

$$\frac{dp}{dt} = -\frac{p - p_\infty}{\tau} \tag{2.5}$$

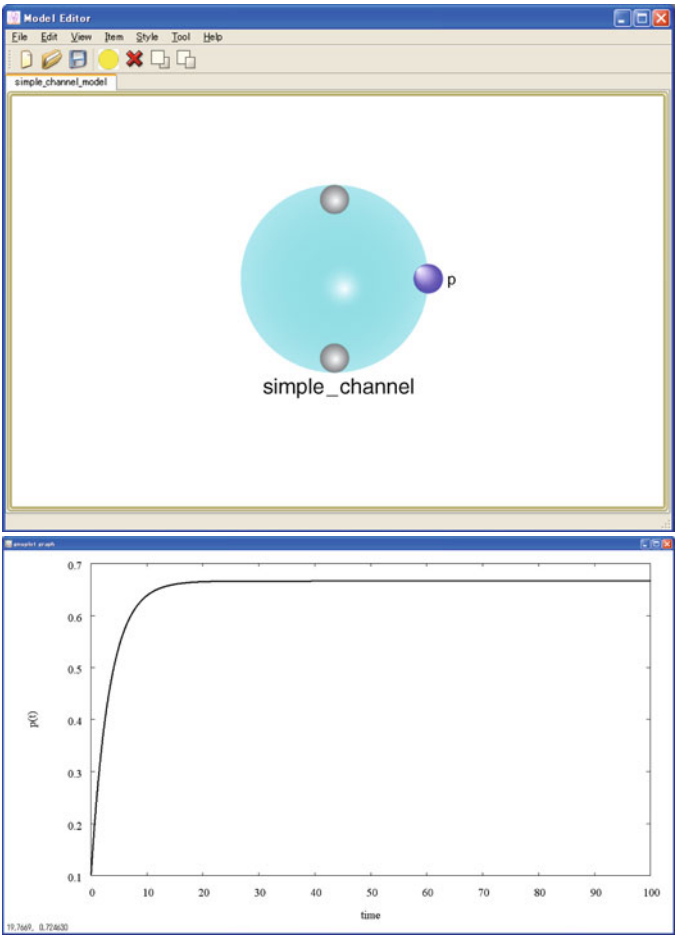


Fig. 2.4 IDE modeling of a simple channel kinetics. *Upper*: Screen shot of the *insilico*IDE platform for the model which is represented as the ball-like module on the canvas. *Lower*: Dynamics of a simple channel model of (2.2) simulated using *insilico*IDE platform. An initial condition is set as $p(0) = 0.1$. The parameter values used here are $k^+ = 0.2$ and $k^{-1} = 0.1$

Figure 2.4 shows a screen snapshot of this model at the upper panel and a numerical solution of (2.2) or (2.5) at the lower panel. We use a tool called the *insilico*IDE of *insilico* platform (see footnote 18). Hereafter in this textbook, we will frequently use this platform provided by *Physiome.jp* at http://www.physiome.jp. It is one of the public efforts for promoting sharing of mathematical models of physiological functions and their related information. It is on the public domain and can be downloaded for free and used for simulating and/or constructing models of physiological functions. The platform also provides a standard format for describing mathematical models of physiological functions. It is based on a XML technology, and the format is called *insilico*ML (*insilico* Markup Language) abbreviated as ISML. A single ISML file includes all information necessary for a numerical simulation of the model

such as equations of the model, text explanation of the model as well as published articles related to the model. See later part of this textbook for details of the ISML format and the *insilico*IDE. In the upper panel of the figure, a ball-like object is displayed on a white canvas of the *insilico*IDE. We call such a ball-like object the *module*, representing a specific physiological function or a set of functions. In this example, the module represents the membrane channel kinetics modeled by (2.5). The module has a site from which the user can obtain internal information of the module called the *out-port* and it is represented as a small circle located on the right edge of the ball-like module. In this example, a value of the state variable $p(t)$ of the model can be obtained through the output port. It is a solution of the model when we use the *insilico*IDE as a model simulator. The lower panel of the figure is obtained in such a way for an initial condition $p(0) = 0.1$ specified in the module. The parameter values of the model are also defined in the module, and in this case, they are $k^+ = 0.2$ and $k^- = 0.1$. The numerical solution asymptotes to 0.66 which is identical to $p_\infty = k^+/(k^- + k^+) = 0.2/(0.2 + 0.1) \sim 0.66$ as predicted by the analytical expression in (2.4). It can be observed from the time course of the solution that the *time constant* of this simple dynamics is $\tau = 1/(k^- + k^+) = 1/(0.2 + 0.1) \sim 3.3$ s. That is, starting from $p(0) = 0.1$ at $t = 0$ s, $e^{-1} \times 100\%$ of the final asymptotic value 0.66 is attained at the time $t = \tau \sim 3.3$ s. The smaller the time constant is, the faster are the dynamics and the shorter is this time interval.

2.2 First Encounter with Numerical Simulations of Ordinary Differential Equations

Equation (2.2) can be discretized as follow.

$$\frac{p(t + \Delta t) - p(t)}{\Delta t} = -\frac{p(t) - p_\infty}{\tau} \equiv f(p(t))$$

Rearranging the discretized equation, we have

$$p(t + \Delta t) = p(t) + \Delta t\, f(p(t))$$

For a given initial condition $p(0)$ at $t = 0$, one can obtain the state variable $p(\Delta t)$ at $t = \Delta t$ as

$$p(\Delta t) = p(0) + \Delta t\, f(p(0)).$$

We repeat the same to have the values of p at $t = 2\Delta t, \ldots, n\Delta t$ as follows:

$$\begin{aligned} p(2\Delta t) &= p(\Delta t) + \Delta t f(p(\Delta t)) \\ &\vdots \\ p(n\Delta t) &= p\left((n-1)\Delta t\right) + \Delta t f(p((n-1)\Delta t)) \end{aligned}$$

This type of simple numerical integration is called the *forward Euler discretization scheme*. Here we consider a very simple ODE

$$\frac{dp}{dt} = -\frac{p}{\tau} \tag{2.6}$$

by setting $p_\infty = 0$ in (2.5) or by the use of the variable transform as $p \to p - p_\infty$ to apply the forward Euler scheme. The iterative applications of the Δt time evolution for a given initial condition $p(0)$ yields

$$\begin{aligned} p(n\Delta t) &= p\left((n-1)\Delta t\right) - \frac{\Delta t}{\tau} p((n-1)\Delta t)) \\ &= \left(1 - \frac{\Delta t}{\tau}\right) p\left((n-1)\Delta t\right) \\ &= \left(1 - \frac{\Delta t}{\tau}\right)^n p(0) \end{aligned}$$

$p(n\Delta t)$ must be converging to zero as $n \to \infty$ for a positive τ, and it is the case if we take Δt smaller than τ. However $p(n\Delta t)$ will show a damped oscillation or oscillatory explosion if we take a large step of time discretization for Δt which makes $(1 - \Delta t/\tau) < 0$, implying a numerical instability.

The derivative of $p(t)$ in (2.2) can also be discretized differently to have the following approximated equation.

$$\frac{p(t) - p(t - \Delta t)}{\Delta t} = f(p(t)).$$

One should avoid a pitfall of taking $p(t - \Delta t)$ for the argument of the function f at the right-hand-side of (2.2). That is, one should note that only $dp(t)/dt$ is approximated differently from the case above. Then we have

$$p(t) = p(t - \Delta t) + \Delta t f(p(t)). \tag{2.7}$$

This is called the *backward (implicit) Euler discretization scheme* to obtain the state variable $p(t)$ at time t from a given $p(t - \Delta t)$ at time $t - \Delta t$, one time step past. In order to obtain the unknown variable $p(t)$ from a known value of $p(t - \Delta t)$, we need to solve (2.7) with respect to $p(t)$. To this end, (2.7) is rearranged as

$$p(t) - \Delta t f(p(t)) = p(t - \Delta t).$$

Let us define a function $G(p(t))$ as

$$G(p(t)) \equiv p(t) - \Delta t f(p(t))$$

to have the algebraic equation

$$G(p(t)) = p(t - \Delta t).$$

Then $p(t)$ can be obtained by solving formally as

$$p(t) = G^{-1}(p(t - \Delta t))$$

if G is locally invertible around $p(t)$. Equivalently, $p(t)$ can be obtained as a solution (zero) of the algebraic equation $G(p(t)) - p(t - \Delta t) = 0$.

For the simple example of (2.6) used above,

$$G(p(t)) \equiv \left(1 + \frac{\Delta t}{\tau}\right) p(t)$$

and we need to solve

$$G(p(t)) = p(t - \Delta t)$$

yields

$$p(t) = \frac{1}{\left(1 + \frac{\Delta t}{\tau}\right)} p(t - \Delta t).$$

Thus

$$p(n\Delta t) = \frac{1}{\left(1 + \frac{\Delta t}{\tau}\right)^n} p(0)$$

which is always converging to zero regardless of the value Δt. This means that the implicit Euler is more robust than the forward Euler in terms of the numerical stability.

2.3 Gating of Ion Channels in the Hodgkin–Huxley Formulation

In 1952, Alan Hodgkin and Andrew Huxley published a paper that summarized essential mechanisms explaining dynamic electrical behaviors of cellular membranes referred to as the *membrane excitation*, that is, to describe the action potential, using squid giant axons (Hodgkin and Huxley 1952). They received the 1963 Nobel Prize in Physiology and Medicine for this work. Their formulation is well-known as the *Hodgkin–Huxley model* (HH model) or the HH equation.

Figure 2.5 illustrates their modeling concept, in which three kinds of ion channels embedded in the axonal membrane are considered. They are the potassium ion channel that is specifically permeable to K^+ ions, the sodium ion channel that is specifically permeable to Na^+ ions, and the chloride ion channel or so called leak channel that is permeable to Cl^- ions.

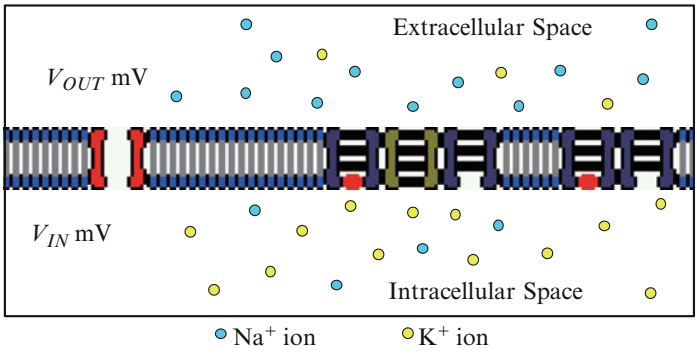


Fig. 2.5 A schematic illustration of ion channel kinetics in the Hodgkin–Huxley formulation

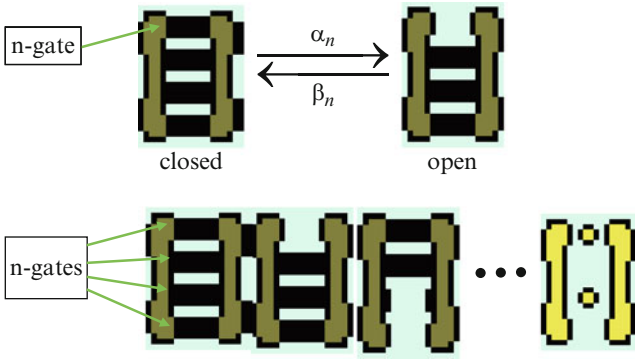


Fig. 2.6 Gating of the potassium channel in the Hodgkin–Huxley formulation

The basic idea of the HH model is the same as the simple channel that we have analyzed for (2.2). However, the open–close kinetics is slightly complicated. Hodgkin and Huxley proposed the concept of *gating* which can describe the opening (activation) or closing (inactivation) of ion channels. In terms of gating, a single channel in (2.2) has a single gate whose opening and closing correspond to the channel opening and closing, respectively. In general, a single ion channel can have several gates. In this case, an open state of the channel is achieved when all of the gates associated with the channel are in their open states.

Let us begin with modeling of the *potassium ion channel*. Hodgkin and Huxley hypothesized that a single potassium channel possesses four identical gates, each of which is referred to as the n-gate. See Fig. 2.6 visualizing this situation in which a cartoon of the single K^+ channel at the top-left corner has four horizontal bars representing four n-gates associated with this channel. The upper part of Fig. 2.6 shows a state transition of the most upper n-gate of the channel where the gate is closed on the left, and it is open on the right. The rate constant for the closed to open transition is α_n, and that for the open to closed is β_n. The HH model assumes the identicality and stochastically independence of four n-gate kinetics for each of

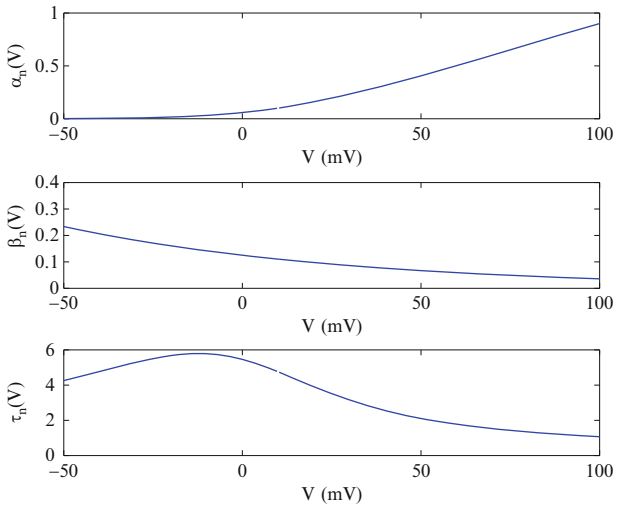


Fig. 2.7 Membrane potential dependency of $\alpha_n(V)$, $\beta_n(V)$ and $\tau_n(V)$ of the n-gate kinetics of the potassium channel

the K^+ channel. Because of the stochastic independence of the gates, opening and closing of one of four gates do not affect that of the other gates. The lower part of Fig. 2.6 shows several different states of the potassium channel. Three situations on the left are all representing closed states where all four gates are closed in the left-most case, the only top gate is open with the other three gates closed in the middle case, and the top and the second gates are closed with the third and the bottom gates open in the right case. There are several combinations for such open–closed gates. The case in which all of four gates are open as illustrated in the right-most cartoon of the lower part of Fig. 2.6 represents the open state of the potassium channel, allowing influx and efflux of potassium ions.

The HH model assumes that the rate "constants" α_n and β_n are not constant, but they change as the functions of the membrane potential V which is the difference in the electrical potential inside and outside the membrane as we will define later in this chapter. As shown in Fig. 2.7, $\alpha_n(V)$ and $\beta_n(V)$ are, respectively, monotonically increasing and decreasing functions of V. Because of this, when the membrane potential V is low, β_n is greater than α_n, allowing more frequent transitions of n-gates from open to closed. Thus the channel is more likely in the closed state. When V is high, α_n is greater than β_n, and it allows n-gates to make more frequent transitions from closed to open. Thus the channel is more likely in the open state.

IDE Modeling: *n*-Gate Model of the HH Potassium Channel: Search ModelDB by "n Gate" to Find n_Gate_Model.isml

$$\frac{dn}{dt} = -\frac{n - n_\infty(V_{clamp})}{\tau_n(V_{clamp})} \tag{2.8}$$

Equation (2.8) represents the n-gate open–close kinetics. Hodgkin and Huxley identified the dynamics of n-gate using an electrophysiological techniques called the *voltage clamp* in which the membrane potential, i.e., the electrical potential difference between inside and outside of the membrane is clamped (fixed). They observed the potassium ion current in response to a step-wise constant clamp voltage. Here we simulate (2.8) to examine dynamic changes in the opening probability of the n-gate in response to a step-wise constant clamp voltage (V_{clamp}). Figure 2.8 shows a modeling of the voltage clamp *in silico* experiment (upper panel) and a numerical solution for (2.8) in response to a step-wise voltage clamp (lower panel). In the upper panel, we have two modules, representing specific functions. The left module represents a voltage step generator and the right module a single n-gate.

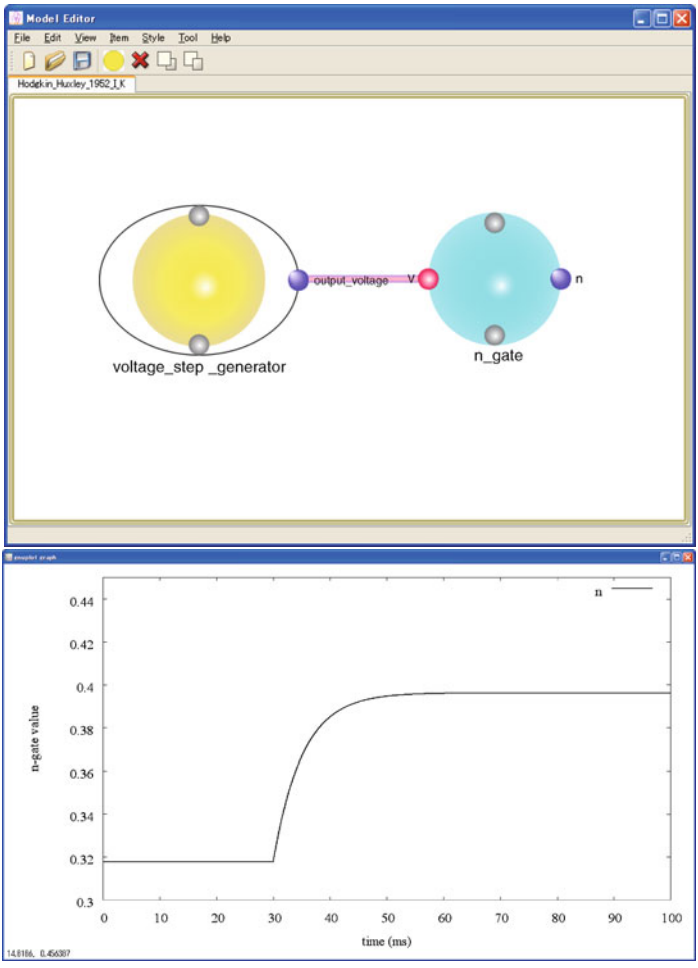


Fig. 2.8 A numerical solution of (2.8) in response to a step-wise voltage clamp. The clamp voltage for the first 30 ms is 0 mV and that after 30 ms is 5 mV. The initial value $n(0)$ is set to $n_\infty(0) \sim 0.32$

The step voltage generated by the left module is delivered to the right module through the line connecting these two modules. The clamp voltage for the first 30 ms is set to 0 mV, and then it becomes $V_{clamp} = 5$ mV after $t = 30$ ms as these parameters are defined in the module of the voltage step generator. The initial value $n(0)$ is set to $n_\infty(0) = \alpha_n(0)/(\alpha_n(0) + \beta_n(0)) \sim 0.32$ in the module representing the n-gate. For the clamp voltage of $V = 5$ mV, $n(t)$ asymptotes to $n_\infty(5) = \alpha_n(5)/(\alpha_n(5) + \beta_n(5))$ which is about 0.4 as shown in Fig. 2.8. As in the case of (2.2), the time constant of the n-gate kinetics is determined by $\tau_n(V_{clamp}) = 1/(\alpha_n(V_{clamp}) + \beta_n(V_{clamp}))$ which stays at a constant value when the voltage is clamped at the fixed value V_{clamp}. As one can read from Fig. 2.7-bottom, $\tau_n(5)$ is about 4 ms, and this value is consistent with the rise time of the step response of the n-gate shown in Fig. 2.8-lower. Note that both $n_\infty(V)$ and $\tau_n(V)$ will be no longer constant if the membrane potential V changes dynamically when we consider action potential generations as we will see later in this chapter.

As in the potassium channel with the n-gate kinetics, the sodium channel kinetics can also be described similarly, but using different types of gates. The HH model assumes two types of gates for Na^+ channel. They are the m-gate and the h-gate. More specifically, Na^+ channel has three m-gates and one h-gate as illustrated in Fig. 2.9.

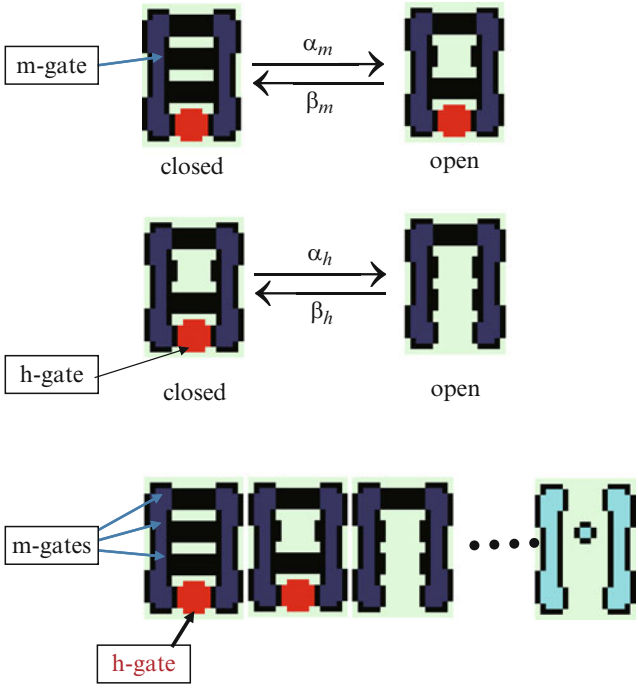


Fig. 2.9 Gating of the sodium channel in the Hodgkin–Huxley formulation. The Na^+ channel of the HH model has three m-gates shown as the *dark horizontal bars* from the *top* to the third position of the channel. It has one h-gate which is located at the *bottom* of the channel in this illustration

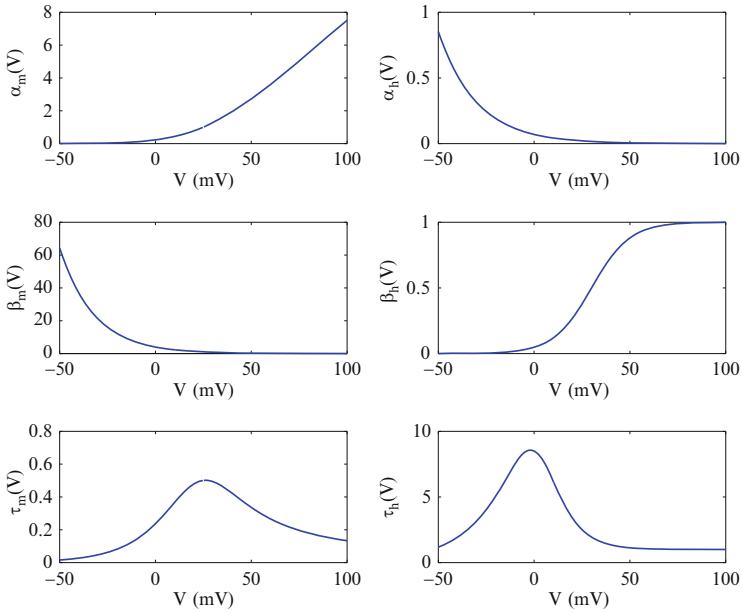


Fig. 2.10 Membrane potential dependency of $\alpha_m(V)$, $\beta_m(V)$ and $\tau_m(V)$ of the m-gate kinetics and $\alpha_h(V)$, $\beta_h(V)$ and $\tau_h(V)$ of the h-gate kinetics for the sodium channel

The m-gate and h-gate have different kinetics. The voltage dependent rate functions determining the transitions between closed and open states of the gates are represented by $\alpha_m(V)$ and $\beta_m(V)$ for each of the m-gates (Fig. 2.9 top row) and by $\alpha_h(V)$ and $\beta_h(V)$ for the h-gate (Fig. 2.9 second row). Note that this diagram at the second row is only for the open–close kinetics of h-gate. That is, open–close of m-gate in this diagram should be neglected. The Na^+ channel is closed at least any one of the four gates is closed as exemplified by three cases in the left part of Fig. 2.9-bottom. It is open if all three m-gates and the h-gate are open, allowing influx and efflux of sodium ions.

As one can observe in Fig. 2.10, $\alpha_m(V)$ and $\beta_m(V)$ are, respectively, monotonically increasing and decreasing functions of V. This is qualitatively the same as the n-gate of the potassium channel. The $\alpha_h(V)$ and $\beta_h(V)$ have opposite characteristics, i.e., the $\alpha_h(V)$ and $\beta_h(V)$ are, respectively, monotonically decreasing and increasing functions of V. When the membrane potential V is low, β_m is greater than α_m, and β_h is smaller than α_h. Thus all m-gates tend to be closed and h-gates tend to be open, implying, in total, that the Na^+ channel tends to be in the closed state for low V. When V is high, α_m is greater than β_m, and α_h is smaller than β_h. Thus the m-gates tend to be open, and the h-gates tend to be closed. Even if all three m-gates are open for a specific single Na^+ channel, the Na^+ channel cannot be in its open state if the h-gate is closed for high values of V. Is there any chance for the Na^+ channel to be open? The answer depends on the dynamics of the m-gate and the h-gate. Here we need to look at the time scales of the m and h gates.

Let us compare the time "constant" functions $\tau_m(V)$ and $\tau_h(V)$ in Fig. 2.10. Although both of them are single humped functions of V, $\tau_h(V)$ is about ten times larger than $\tau_m(V)$ for any value of V. This means that the open–close dynamics of the h-gate are about ten times slower than those of the m-gate. That is, for an increase in the membrane potential from a low potential value for which the h-gates are mostly open, the m-gates open rapidly, leading to the open state of the sodium channel. Then h-gates and thus the sodium channel begins to be closed.

IDE Modeling: *n-m-h* Gating Dynamics with Voltage Clamp: Search ModelDB by "gate" to Find nmh_Gating_Dynamics.isml

$$\begin{aligned}\frac{dn}{dt} &= -\frac{n - n_\infty(V_{clamp})}{\tau_n(V_{clamp})}\\ \frac{dm}{dt} &= -\frac{m - m_\infty(V_{clamp})}{\tau_m(V_{clamp})}\\ \frac{dh}{dt} &= -\frac{h - h_\infty(V_{clamp})}{\tau_h(V_{clamp})}\end{aligned} \tag{2.9}$$

This IDE model compares the time scales of the n-gate, the m-gate, and the h-gate in response to a step-wise voltage clamp common to these three gate variables by simulating a set of three gating equations in (2.9). This can be modeled on *insilico*IDE by preparing these gating models on the canvas and then providing the output signal of the voltage step generator to each of the gating models as shown in Fig. 2.11 upper panel. The clamp voltage for the first 30 ms is 0 mV and that after 30 ms is $V_{clamp} = 20$ mV. The initial values $n(0)$, $m(0)$, and $h(0)$ are set to $n_\infty(0) \sim 0.32$, $m_\infty(0) \sim 0.05$, and $h_\infty(0) \sim 0.59$, respectively. As shown in Fig. 2.11 lower panel, in response to a step change in the clamp voltage, the m-gate increases (opening of the m-gate) rapidly with its time constant $\tau_m(V_{clamp}) = 1/(\alpha_m(V_{clamp}) + \beta_m(V_{clamp}))$ which is about 0.3 ms, followed by the slow increase in the n-gate (opening of the n-gate) and the slow decrease in the h-gate (closing of the h-gate). Thus, the Na^+ channel takes its open state for a short interval between the onset of the step-change in the clamp voltage until the h-gate is closed with its time constant $\tau_h(V_{clamp}) = 1/(\alpha_h(V_{clamp}) + \beta_h(V_{clamp}))$ which is about 5 ms.

2.3.1 Electro-Chemical Potentials for Cell Membranes

Cells contain relatively high concentration of potassium ions K^+ and low concentration of sodium ions Na^+. This situation is established by the mechanism called the *sodium–potassium pump*. The Na^+/K^+ pump actively moves Na^+ and K^+ ions in opposite directions across the membrane, in which three sodium ions are pumped out, and, at the same time, two potassium ions are pumped in. An enzyme called

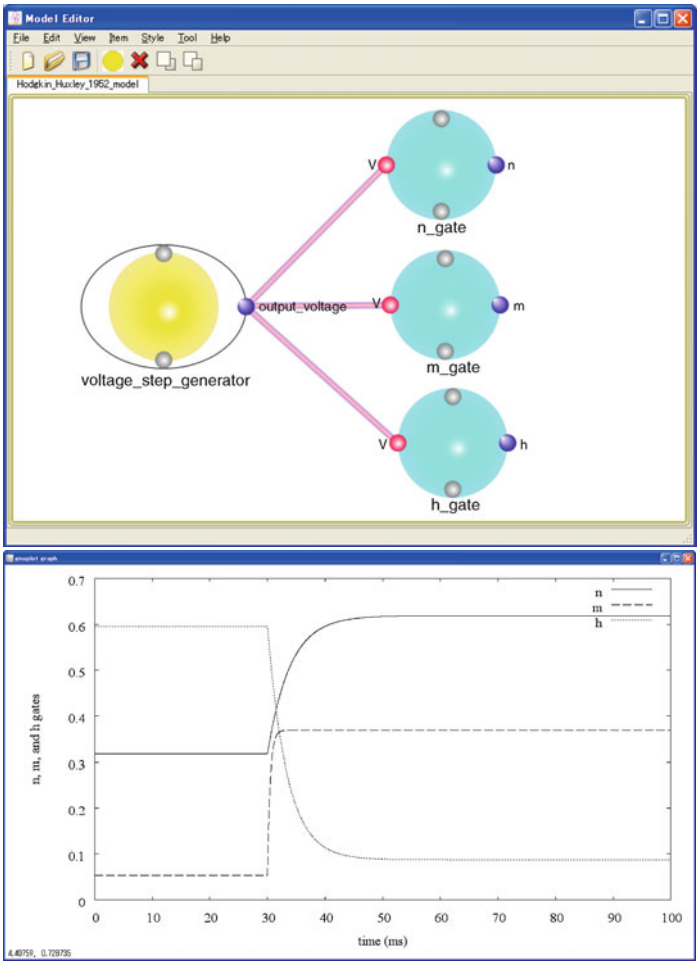


Fig. 2.11 *Upper panel*: The *n*-*m*-*h* gate models on *insilico*IDE with the voltage step generator driving the gate models. *Lower panel*: A numerical solution of (2.9) in response to a step-wise voltage clamp. The clamp voltage for the first 30 ms is 0 mV and that after 30 ms is 20 mV. The initial values of $n(0)$, $m(0)$, and $h(0)$ are set to $n_\infty(0) \sim 0.32$, $m_\infty(0) \sim 0.05$, and $h_\infty(0) \sim 0.59$, respectively

Na^+/K^+-ATPase embedded in the membrane is responsible for this pump. Because of this mechanism, the intra-cellular K^+ concentration is kept higher than the extra-cellular K^+ concentration and the intra-cellular Na^+ concentration is kept lower than the extra-cellular Na^+ concentration as illustrated in Fig. 2.12.

When solute ions with different concentrations are separated by the membrane that is permeable to this specific type of ion, the ions move or diffuse across the membrane according to the concentration gradient so that the concentrations are equalized or equilibrated. The statistical mechanics explains this using "a force" whose potential energy is known as *chemical potential*. The diffusion induced by

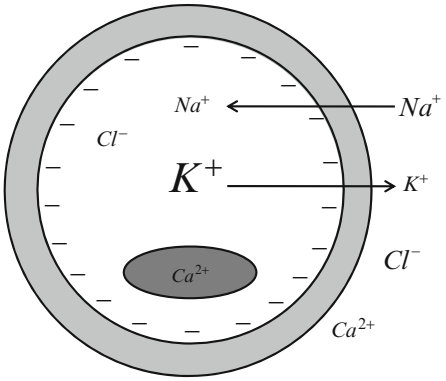


Fig. 2.12 Intracellular and extracellular spaces

the concentration gradient can also be modeled by Fick's law. Here we consider a one-dimensional space x with a unit of m (meter), which may correspond here to the direction normal to the membrane. In this case, *Fick's law* relates the diffusive flux with a unit of mol/(m^{2}s) to the spatial gradient of the concentration as follows;

$$J_c = -D\frac{dC}{dx} \tag{2.10}$$

where J_c represents the flux, which is the amount of the ion that will flow through a unit area within a unit time interval, D the diffusion coefficient with a unit of m^2/s, and C the concentration of the ion with a unit mol/m^3. This just says that the flow is proportional to the intensity of the concentration gradient.

If the ion is electrically charged with its valence z, the electrical force and its potential is also involved. The flow of ions across the membrane is thus driven by concentration gradients and by the electric field. The electric contribution to the flow is determined by *Planck's equation* as follows;

$$J_e = -u\frac{z}{|z|}C\frac{d\phi}{dx} \tag{2.11}$$

where J_e represents the flux induced by the electric field, which is the amount of the charged ion that will flow through a unit area within a unit time interval, u the mobility with a unit of m^2/(Vs), C the concentration of the ion with a unit mol/m^3 as above, and ϕ the electric potential. $z/|z|$ determines the valence-dependent direction of the flow. The mobility u may depend, for example, on the size of the ion. Small (large) ions are easy (hard) to move, leading to a large (a small) mobility. Ions in a viscous liquid may have a small mobility. The Planck's equation just also says that the flow is proportional to the intensity of the electric potential gradient, i.e., the electric field as well as the concentration of the charged ion.

Let us just use, without getting into details, the following relationship (Kubo 1966)

$$D = \frac{uRT}{|z|F} \tag{2.12}$$

which connects the mobility u with the diffusion constant D, where R is the universal gas constant with a unit of J/(K mol), and T the absolute temperature in Kelvin, or equivalently

$$u = D\frac{|z|F}{RT}.$$

Then, the total flow of the ion, J, that is transverse to the membrane in the direction of x can be described as;

$$J = J_c + J_e = -D\left(\frac{dC}{dx} + \frac{zF}{RT}C\frac{d\phi}{dx}\right). \tag{2.13}$$

At the electro-chemical equilibrium where the electro-chemical forces are balanced between two sides of the membrane, the net flux J is zero. Thus we obtain

$$-D\left(\frac{dC}{dx} + \frac{zF}{RT}C\frac{d\phi}{dx}\right) = 0, \tag{2.14}$$

so that

$$\frac{1}{C}\frac{dC}{dx} + \frac{zF}{RT}\frac{d\phi}{dx} = 0. \tag{2.15}$$

Let us denote the concentration of the ion inside and outside the membrane, respectively, C_i and C_o, and the electrical potential inside and outside the membrane, respectively, ϕ_i and ϕ_o with assuming that these potentials are constant at either side of the membrane. For any points x_i and x_o inside and outside the membrane, respectively,

$$\int_{x_i}^{x_o} \frac{1}{C(x)}\frac{dC(x)}{dx}dx = -\frac{zF}{RT}\int_{x_i}^{x_o}\frac{d\phi(x)}{dx}dx,$$

which can be rewritten as

$$\int_{C_i}^{C_o} \frac{1}{C(x)}dC(x) = -\frac{zF}{RT}\int_{\phi_i}^{\phi_o} d\phi(x),$$

which yields

$$[\ln C(x)]_{C_i}^{C_o} = \frac{zF}{RT}(\phi_i - \phi_o). \tag{2.16}$$

The electrical potential difference across the membrane is called the *membrane potential*, and we define it as $V = \phi_i - \phi_o$. If we denote the membrane potential V at this equilibrium specifically as E, then (2.16) becomes

$$E = \frac{RT}{zF}\ln\left(\frac{C_o}{C_i}\right). \tag{2.17}$$

Equation (2.17) is called the *Nernst equation*, and E is referred to as the *Nernst potential*.

Much more thorough considerations on this and related issues are available in many literatures such as the one by Keener and Sneyd (2009).

Exercise 2.2. Consider the following intracellular and extracellular ion concentrations. $[K^+]_i = 150\,\text{mM}$, $[K^+]_o = 5\,\text{mM}$, $[Na^+]_i = 15\,\text{mM}$, and $[Na^+]_o = 135\,\text{mM}$. Physical constants are given as $F = 96,500\,\text{C/mol}$, $R = 8.31\,\text{J/mol/K}$, and assume $T = 300\,\text{K}$. Estimate the Nernst potentials for K^+ and Na^+ in the unit of mV.

2.3.2 Electric Circuit Model of Cell Membranes

The flow of ions across the membrane can be viewed as the current. They flow through the channel dominantly, but some part of it is contributed by the capacitant property of the membrane (the lipid bilayer). Because of the capacitant property of the lipid bilayer, it is electrically polarized. The outer and inner surfaces of the membrane are positively and negatively charged, respectively. That is, the membrane as the capacitant stores an amount of electric charge q (Coulomb). With this property, the current–voltage relationship of a cell can be modelled as Fig. 2.13, in which two terminals of the circuit correspond to the inside and the outside of the membrane whose electrical potentials are ϕ_i and ϕ_o, and the difference between them is $V = \phi_i - \phi_o$, the membrane potential. In Fig. 2.13, the outside of the membrane is taken as the ground, i.e., $\phi_o = 0$.

Here, for simplicity, we consider only a single type of the channel through which only a single type of ions flows. The amount of the ionic current may depend on the open fraction of the gates of the channel. The larger the open fraction, the larger is the current. This dependency can be modeled as the resistance R (Ohm) or the

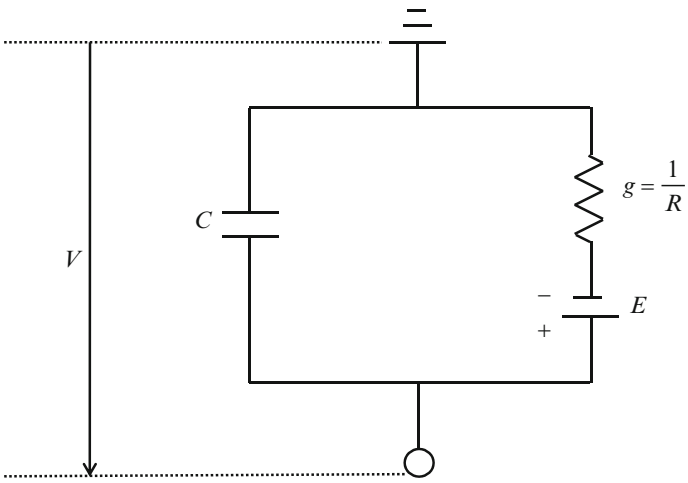


Fig. 2.13 A simple analog electric circuit with resistance and capacitance

conductance $g = 1/R$ (S) of the circuit. A large conductance (or a small resistance) implies the large open fraction of the channel gate. The battery E in Fig. 2.13 corresponds to the Nernst potential for this type of the ion. It drives the channel current if the membrane potential V is deviated from the Nernst potential E.

Using the Ohm's law for the circuit on the right of Fig. 2.13 with its current i_R, the law of Frady for the circuit on the left of Fig. 2.13 with its current i_C, and the Kirchhoff's laws, for a given amount of externally applied current I_{ext}, we have

$$\begin{aligned} i_R &= g(V - E), \\ q &= CV, \text{ or } i_C \equiv \frac{dq}{dt} = C\frac{dV}{dt}, \\ I_{ext} &= i_R + i_C, \end{aligned}$$

yielding the differential equation that governs dynamic change of the voltage difference between the reference and the other side of this RC circuit as follows:

$$C\frac{dV}{dt} = -g(V - E) + I_{ext}, \tag{2.18}$$

where I_{ext} represents the externally injected current. Note that the resistance (conductance) current i_R corresponds to the channel current.

When I_{ext} is constant, using a variable transform as $v = V - E - I_{ext}/g$, (2.18) can be rewritten as

$$\frac{dv}{dt} = -\frac{v}{RC} \tag{2.19}$$

which has exactly the same form as (2.6), and can be solved analytically. Note also that the time constant of the dynamics is RC.

2.4 Hodgkin–Huxley Formulation of Membrane Excitation

As in the electric circuit model described above in (2.18), Hodgkin and Huxley proposed a model of the current through the sodium channel as

$$I_{Na} = \bar{g}_{Na} m^3 h (V - E_{Na}) \tag{2.20}$$

where I_{Na} represents the sodium current through all of the Na^+ channels embedded in the membrane, E_{Na} the Nernst potential for the Na^+ ions, and $\bar{g}_{Na} m^3 h$ the conductance determined by all Na^+ channels with the gate variables m and h defined previously. Since m and h are the open fractions of the gates when we consider the whole gates in the membrane (and they are the open probability when we consider a specific single channel), they take values between 0 and 1. When all of m and h gates are open, $m = h = 1$, implying the conductance of the sodium channel is $\bar{g}_{Na}$ representing the maximum conductance (the minimum resistance). When all of m

and h gates are closed, $m = h = 0$, implying the conductance of the sodium channel is zero. This means that the resistance of the channel is infinity. In summary, the amount of the sodium current is proportional to the conductance $\bar{g}_{Na}m^3h$ and also to the electric potential $V - E_{Na}$.

Let us consider the form of m^3h for the sodium channel conductance. It reflects the fact that we have modeled the sodium channel with three m-gates and single h-gate. The term m^3 represents the probability that, for a specific channel, all of its three m-gates are open. This is true because we have assumed that the open–close transition of every m-gate is independent of the other m-gates. By the same reason, the m^3 also represents the fraction in the number of the channels for which all three m-gates are open. Together with the h-gate, the term m^3h represents the probability that, for a specific channel, all of its three m-gates and its single h-gate are open. Similarly, the m^3h also represents the fraction in the number of the channels for which all three m-gates and one h-gate are open.

In a similar way, the potassium channel current of the HH model is formulated as

$$I_K = \bar{g}_K n^4 (V - E_K) \tag{2.21}$$

where I_K represents the potassium current through all of the K^+ channels embedded in the membrane, E_K the Nernst potential for the K^+ ions, and $\bar{g}_K n^4$ the conductance for all K^+ channels with the gate variables n defined previously.

The HH model includes three currents. The last one is the leak current I_L which is hypothetized conducting Cl^- ions. The conductance of I_L is assumed as a constant $\bar{g}_L$ which does not depend on the membrane potential, and thus I_L is formulated as

$$I_L = \bar{g}_L (V - E_L) \tag{2.22}$$

where E_L is the Nernst potential of Cl^-.

IDE Modeling: Voltage Clamp Experiment for I_{Na} Current of the HH: Search ModelDB by "Sodium Current" to Find HH_Sodium_Current_Clamp.isml

$$\begin{aligned} I_{Na} &= \bar{g}_{Na} m^3 h (V_{clamp} - E_{Na}) \\ \frac{dm}{dt} &= -\frac{m - m_\infty(V_{clamp})}{\tau_m(V_{clamp})} \\ \frac{dh}{dt} &= -\frac{h - h_\infty(V_{clamp})}{\tau_h(V_{clamp})} \end{aligned} \tag{2.23}$$

The electrical potential inside the membrane can be fixed at a constant using a voltage clamp technique. The HH model was derived using such a voltage clamp experiment. Here we simulate (2.23) as in the previous examples of IDE modeling. On the *insilico*IDE, we set two modules representing the voltage step generator and the I_{Na} current of the HH as shown in the upper panel of Fig. 2.14. The initial clamp

voltage V_{clamp} is zero, and at $t = 30$ ms, the clamp voltage is re-set to $V_{clamp} = 20$ mV. We simulate a response of the Na^+ current to this step change using *insilico*IDE to obtain a transient rapid increase of I_{Na} in the negative direction (inward current) and then relatively slow decrease of the current as shown in Fig. 2.14-lower panel. According to our consideration so far on the gate dynamics, the rapid increase of the current is induced by the rapid opening of the m-gates in response to the onset of the step, and the decrease of the current is by the relatively slow closing of the h-gate. Since the voltage is constant after $t = 30$ ms, the second and the third ODEs in (2.23) can also be solved analytically for $t > 30$ as in (2.4);

$$\bar{m}(t) = m(30)\exp\left(-\frac{t-30}{\tau_m(V_{clamp})}\right) + m_\infty(V_{clamp})\left(1-\exp\left(-\frac{t-30}{\tau_m(V_{clamp})}\right)\right)$$

$$\bar{h}(t) = h(30)\exp\left(-\frac{t-30}{\tau_h(V_{clamp})}\right) + h_\infty(V_{clamp})\left(1-\exp\left(-\frac{t-30}{\tau_h(V_{clamp})}\right)\right)$$

Thus we are able to obtain an analytical expression of the step response of I_{Na} as;

$$I_{Na}(t) = \bar{g}_{Na}\bar{m}^3(t)\bar{h}(t)(V_{clamp} - E_{Na}).$$

as the function of time $t > 30$.

The HH model can be summarized as a set of ordinary differential equations as follows;

$$\begin{aligned}
C\frac{dV}{dt} &= -\bar{g}_{Na}m^3h(V-E_{Na}) - \bar{g}_K n^4(V-E_K) - \bar{g}_L(V-E_L) + I_{ext}\\
\frac{dm}{dt} &= \alpha_m(V)(1-m) - \beta_m(V)m\\
\frac{dh}{dt} &= \alpha_h(V)(1-h) - \beta_h(V)h\\
\frac{dn}{dt} &= \alpha_n(V)(1-n) - \beta_n(V)n
\end{aligned} \tag{2.24}$$

By fitting experimental data, Hodgkin and Huxley obtained:

$$\begin{cases}
\alpha_m(V) = 0.1\dfrac{-V+25}{\exp(\frac{-V+25}{10})-1}, & \beta_m(V) = 4\exp\left(-\dfrac{V}{18}\right)\\
\alpha_h(V) = 0.07\exp\left(-\dfrac{V}{20}\right), & \beta_h(V) = \dfrac{1}{\exp(\frac{-V+30}{10})+1}\\
\alpha_n(V) = 0.01\dfrac{-V+10}{\exp(\frac{-V+10}{10})-1}, & \beta_n(V) = 0.125\exp\left(-\dfrac{V}{80}\right)
\end{cases} \tag{2.25}$$

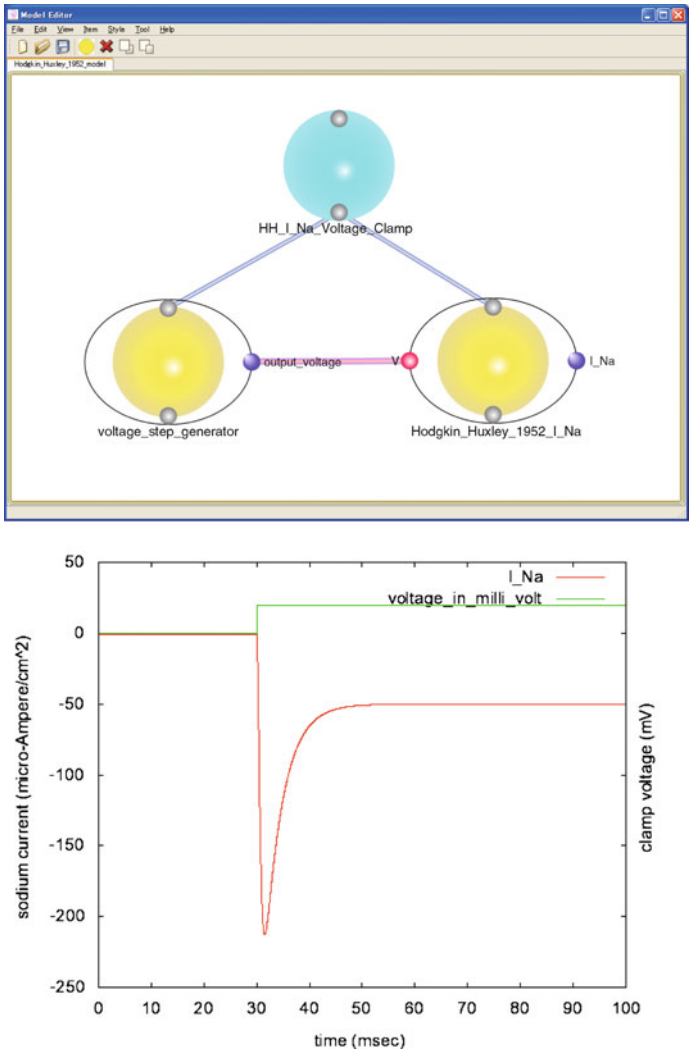


Fig. 2.14 A snapshot of insilicoIDE for a voltage clamp experiment for the HH sodium current, and its simulation outcome

where

I_{ext}	externally applied current [μA/cm^2]
V	intracellular potential measured from the resting potential, positive for the depolarization side [mV]
t	time [ms]
m	sodium activating variable (dimensionless $0 < m < 1$)
h	sodium inactivating variable (dimensionless $0 < h < 1$)
n	potassium activating variable (dimensionless $0 < n < 1$)
C	membrane capacitance [$= 1\mu$ F/cm^2]

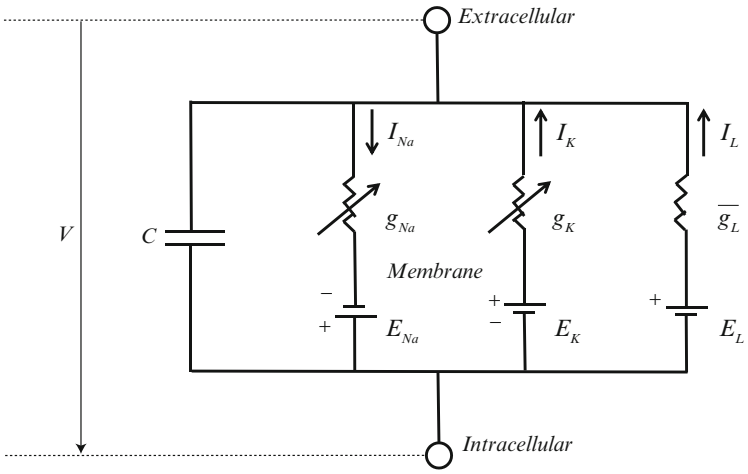


Fig. 2.15 Equivalent electric circuit model of a cellular membrane after Hodgkin and Huxley

E_{Na} sodium equilibrium potential [$= 115\,\text{mV}$]
E_K potassium equilibrium potential [$= -12\,\text{mV}$]
E_L leak equilibrium potential [$= 10.613\,\text{mV}$]
$\bar{g}_{Na}$ maximum sodium conductance [$= 120\,\text{mS}^{-1}/\text{cm}^2$]
$\bar{g}_K$ maximum potassium conductance [$= 36\,\text{mS}^{-1}/\text{cm}^2$]
$\bar{g}_L$ leak conductance [$= 0.3\,\text{mS}^{-1}/\text{cm}^2$]

Figure 2.15 represents the electric circuit model of the HH. Although the circuit includes three channel currents (I_{Na}, I_K, and I_L) all in parallel with the capacitance, it is conceptually the same as the simple circuit of Fig. 2.13.

Let us consider an equilibrium of the HH model before looking at dynamic behaviors of the model. By the equilibrium, we mean a state where a net current, i.e., the sum of all currents, across the membrane is zero so that the membrane potential stays at a constant value referred to as the *resting potential*. Denoting the resting potential as $\bar{V}$, we have

$$\frac{d\bar{V}}{dt} = 0.$$

At the equilibrium, the other dynamic variables, i.e., m, h, and n, do not also change in time, and they stay at, respectively, $\bar{m}$, $\bar{h}$, and $\bar{n}$. Thus,

$$\frac{d\bar{m}}{dt} = 0,$$

$$\frac{d\bar{h}}{dt} = 0,$$

$$\frac{d\bar{n}}{dt} = 0.$$

Therefore, from (2.24), we have

$$-\bar{g}_{Na}\bar{m}^3\bar{h}(\bar{V}-E_{Na})-\bar{g}_K\bar{n}^4(\bar{V}-E_K)-\bar{g}_L(\bar{V}-E_L)+I_{ext}=0, \quad (2.26)$$

$$\alpha_m(\bar{V})(1-\bar{m})-\beta_m(\bar{V})\bar{m}=0, \quad (2.27)$$

$$\alpha_h(\bar{V})(1-\bar{h})-\beta_h(\bar{V})\bar{h}=0, \quad (2.28)$$

$$\alpha_n(\bar{V})(1-\bar{n})-\beta_n(\bar{V})\bar{n}=0. \quad (2.29)$$

From (2.27) to (2.29), we have

$$\bar{m}=\frac{\alpha_m(\bar{V})}{\alpha_m(\bar{V})+\beta_m(\bar{V})}\equiv m_\infty(\bar{V}) \quad (2.30)$$

$$\bar{h}=\frac{\alpha_h(\bar{V})}{\alpha_h(\bar{V})+\beta_h(\bar{V})}\equiv h_\infty(\bar{V}), \quad (2.31)$$

$$\bar{n}=\frac{\alpha_n(\bar{V})}{\alpha_n(\bar{V})+\beta_n(\bar{V})}\equiv n_\infty(\bar{V}). \quad (2.32)$$

Moreover, together with (2.26), we have

$$I_{ext}=\bar{g}_{Na}m_\infty(\bar{V})^3h_\infty(\bar{V})(\bar{V}-E_{Na})+\bar{g}_Kn_\infty(\bar{V})^4(\bar{V}-E_K)+\bar{g}_L(\bar{V}-E_L) \quad (2.33)$$

For a given constant value of I_{ext}, i.e., for a given direct external current injection, one can solve the nonlinear algebraic equation of (2.33) to obtain the unknown resting potential $\bar{V}$. In particular, when $I_{ext}=0$, we have

$$\bar{V}=\frac{G_{Na}E_{Na}+G_KE_K+G_LE_L}{G_{Na}+G_K+G_L} \quad (2.34)$$

where

$$\begin{aligned} G_{Na} &= \bar{g}_{Na}m_\infty(\bar{V})^3h_\infty(\bar{V}),\\ G_K &= \bar{g}_Kn_\infty(\bar{V})^4,\\ G_L &= \bar{g}_L. \end{aligned}$$

The resting potential $\bar{V}$ for a given I_{ext} constant can also be obtained graphically by numerically plotting I_{ext} as a function of $\bar{V}$ using (2.33). Reversing the plot to have $\bar{V}$ as a function of I_{ext} will be used to determine the resting potential for a given I_{ext}.

IDE Modeling: The Hodgkin–Huxley Model: Search ModelDB by "Huxley" to Find Hodgkin_Huxley_1952_Model.isml

$$
\begin{aligned}
C\frac{dV}{dt} &= -\bar{g}_{Na}m^3h(V-E_{Na}) - \bar{g}_K n^4(V-E_K) - \bar{g}_l(V-E_L) + I_{ext}(t) \\
\frac{dm}{dt} &= -\frac{m-m_\infty(V)}{\tau_m(V)} \\
\frac{dh}{dt} &= -\frac{h-h_\infty(V)}{\tau_h(V)} \\
\frac{dn}{dt} &= -\frac{n-n_\infty(V)}{\tau_n(V)}
\end{aligned}
\tag{2.35}
$$

This IDE modeling examines the action potential generation in the HH model in response to a single and periodic current pulse stimulations. Equation (2.35) is the same as (2.24), but the right-hand-sides of the ODEs for the gate dynamics are rewritten differently. Figure 2.16-upper shows a snapshot of the IDE modeling of the HH, in which the output of the module representing the periodic current pulse generator (corresponding to the external current I_{ext}) is connected to the module representing the HH model. Here the internal structure of the HH model module is also presented. As described in the later part of this book, an IDE module can represent a tree-like hierarchical structure of modules. This is such an example showing that the HH model is consist of the one module representing the membrane or the membrane potential which is further consist of three modules representing the sodium current, the potassium current, and the leak current. In this case, modules at lower layer of the HH model, up to the ion current level, are expanded and shown. Note that each module representing each of three ion currents has further lower layer modules that represent the gates of the channel. Figure 2.16-middle shows the membrane potential response to a single current pulse injected at time $t = 10$ ms with the accompanied dynamics of the m, h, n gates. The rapid and transient increase of the membrane potential is referred to as the *action potential* as well as the *membrane excitation*. It can be observed that the rapid upstroke (opening) of the m-gate corresponds to the onset of the action potential. The decrease in the membrane potential is caused by the decrease (closing) of the h-gate as well as the increase (opening) of the n-gates, both of which changes slower than the m-gate dynamics as we have analyzed based on the values of the τ_m, τ_h, and τ_n. Note that the opening of the m and h gates induces an inward sodium current $I_{Na} = \bar{g}_{Na}m^3h(V-E_{Na})$ because of the electro-chemical potential (the Nernst potential) of the sodium ions, leading to the increase in the membrane potential. Since $I_K = \bar{g}_K n^4(V-E_K)$ and the Nernst potential of the K^+ ions is opposite to the Na^+ ions, the opening of the n-gates induces an outward current of the potassium ions, leading to the decrease in the membrane potential. Figure 2.16-lower shows a sequence of action potentials in response to the periodic current pulse injections. The full-size action potential is generated in response to the first pulse. The response to

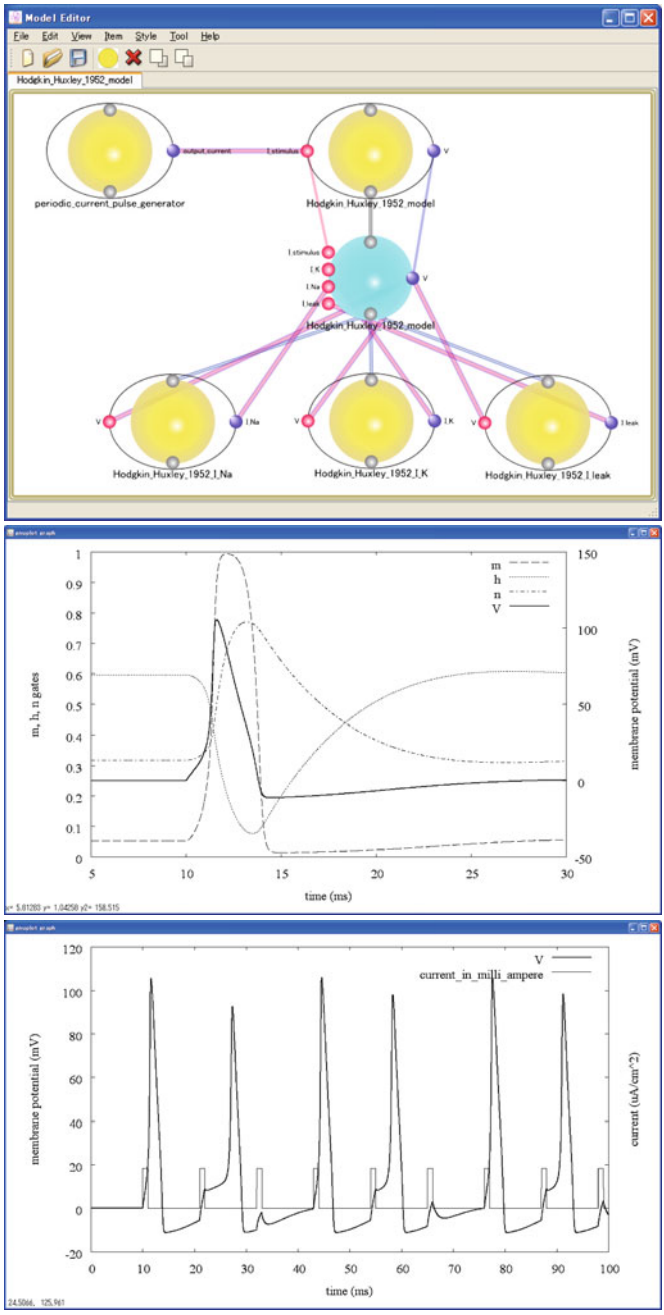


Fig. 2.16 *Upper*: A snapshot of *insilico*IDE for the HH model with pulsatile current injection denoted as $I_{ext}(t)$. *Middle*: An action potential (*solid curve*) in response to a single pulse current with the dynamics of the m-gate (*dashed*), the h-gate (*dotted*), and the n-gate (*dot-dashed*). *Lower*: A response to periodic current pulse stimulations. The period of the pulse sequence for the lower panel is 11 ms. The width and the height of each pulse are 1.0 and 18.445 $\mu A/cm^2$

the second pulse is slightly delayed, and the size of the action potential is slightly smaller than the first one. The third pulse fails to generate the action potential, and so on for the successive current pulses. The delayed response and the failure of the action potential generation are due to the *refractoriness* property of the membrane excitation. That is, once the membrane excites, *excitability* of the membrane decreases for a certain time interval. This is due to the slow recovery dynamics of the h-gate and the n-gate as can be seen from Fig. 2.16-middle. When the h and n gates are recovered, the membrane regains its excitability, allowing full-size action potential responses. The membrane potential at the down-stroke of the action potential goes further below the steady state value that was taken before the action potential generation. This is referred to as *after hyperpolarization* for which the slow closing (inactivation) of the K^+ channel with its slow outward current is responsible.

2.5 FitzHugh–Nagumo Model

Mathematical abstraction of a membrane excitation has been performed by a number of researchers. The most popular one is so-called *FitzHugh–Nagumo (FHN) model* or originally Bonhoeffer–van der Pol (BVP) model (FitzHugh 1961).

$$\begin{aligned} \frac{dv}{dt} &= -v(v-a)(v-b) - w + I_{ext} \\ \frac{dw}{dt} &= \epsilon(v - cw) \end{aligned} \tag{2.36}$$

where $a = 0.139$, $b = 1$, $c = 2.54$, and $\epsilon = 0.008$. The dynamic variables v and w conceptually represent the membrane potential and the refractoriness of the membrane with arbitrary physical units, respectively. I_{ext} represents the externally applied current stimulation.

2.5.1 *More About Numerical Integrations of Ordinary Differential Equations*

We have looked at the forward and backward Euler methods for numerical integrations, i.e., numerical simulations of ordinary differential equations. Here let us consider them in a more general framework using the FHN model. To this end, (2.36) with $I_{ext} = 0$ is rewritten in a vector form as;

$$\frac{d}{dt}\begin{pmatrix} v \\ w \end{pmatrix} = \begin{pmatrix} -v(v-a)(v-b) - w \\ \epsilon(v - cw) \end{pmatrix} \equiv \begin{pmatrix} f_1(v,w) \\ f_2(v,w) \end{pmatrix} \tag{2.37}$$

More abstraction can be performed by defining $x = (v, w)^T$ and $f(x) = (f_1(x), f_2(x))^T$ to have

$$\frac{dx}{dt} = f(x). \tag{2.38}$$

x is referred to as the *state point* of the model. The state point of the FHN is a two-dimensional vector $x = (v, w)^T$. (As another example, the state point of the HH model is a four-dimensional vector whose components are V, m, h, and n.) For the FHN, the two-dimensional space (plane) of x spanned by v and w is referred as the *phase space* (the *phase plane*) if and only if any point in the space (plane) can uniquely specify a state of the model. As we have seen for the HH model, the equilibrium state of the FHN model at which $dx/dt = 0$ satisfies the following algebraic equation;

$$f(x) = 0. \tag{2.39}$$

A vector-component-wise representation of (2.39) for the FHN is

$$-v(v-a)(v-b) - w = 0 \tag{2.40}$$

$$\epsilon(v - cw) = 0 \tag{2.41}$$

In the $v-w$ phase plane, (2.40) represents the cubic curve $w = -v(v-a)(v-b)$ on which dv/dt is always zero. A set of points consisting this curve is referred to as the *v-nullcline*. Similarly, (2.40) represents the straight line $w = v/c$ on which dw/dt is always zero. A set of points consisting this line is referred to as the *w*-nullcline. See Fig. 2.17 for graphical representation of them. The equilibrium state $\bar{x} = (\bar{v}, \bar{w})^T$ is an intersectional point of these two nullclines. Note that, since *v*-nullcline is nonlinear curve in this model, two nullcline can intersect at multiple points (two or three points at most). In such a case, the model has two or three equilibrium points.

One can see a number of arrows in Fig. 2.17. Each of these arrows is defined for a state point located at the origin of the arrow. More precisely, for any state point x on

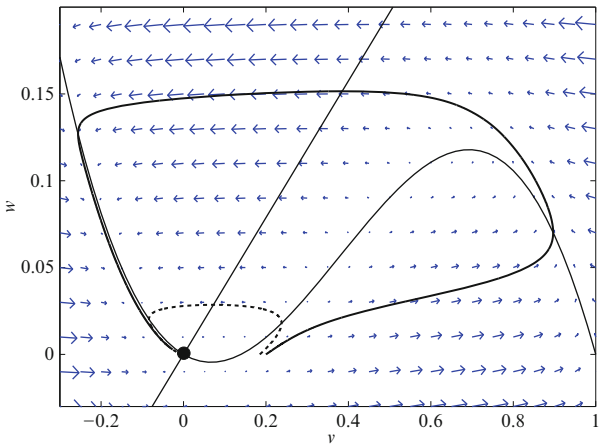


Fig. 2.17 A phase portrait of the FHN model. The cubic shaped *v*-nullcline, straight-line *w* nullcline, the equilibrium point (*closed circle*), and the vector field of the FHN model are shown. Two solution curves started from initial states close to each other are also displayed. One with the *thick curve* moves right-ward corresponding to the onset of the action potential followed by a transient round excursion, eventually settling back to the equilibrium point. In the other with the *dashed curve*, the membrane potential v does not increase corresponding to a subthreshold behavior

the phase plane, its arrow is calculated as $f(x)$ which is defined as the left-hand-side of the ODE of (2.38). Such a set of vectors distributed in the phase space is called the *vector field*. As we have studied, the forward Euler scheme with its time step Δt integrates (2.38) to obtain $x(t + \Delta t)$ from a state point $x(t)$ at time t as follows.

$$x(t + \Delta t) = x(t) + \Delta t \cdot f\left(x(t)\right). \tag{2.42}$$

This equation means that the state point $x(t)$ moves in the direction of the vector field $f(x(t))$ at $x(t)$ by the amount of $\Delta t \cdot f(x(t))$ to reach at $x(t+\Delta t)$. The smaller the time step Δt, the smaller is the amount of the one step movement, providing better approximation of the real solution of (2.38). In other words, if the time step Δt is not small enough, the numerical solution may be very different from the real solution.

There are many methods for the numerical integration of ordinary differential equations. The fourth-order Runge–Kutta method can provide a better approximation than the forward Euler for a given time step Δt. It is formulated as follows.

$$x(t + \Delta t) = x(t) + \frac{1}{6}\Delta t\left(k_1 + 2k_2 + 2k_3 + k_4\right) \tag{2.43}$$

where

$$\begin{aligned} k_1 &= f\left(x(t)\right) \\ k_2 &= f\left(x(t) + \frac{1}{2}\Delta t k_1\right) \\ k_3 &= f\left(x(t) + \frac{1}{2}\Delta t k_2\right) \\ k_4 &= f\left(x(t) + \Delta t k_3\right) \end{aligned}$$

This method is a fourth-order, meaning that the error per one time step is on the order of $(\Delta t)^5$, and, as it can be shown, the total accumulated error has order of $(\Delta t)^4$. The one step movement in the forward Euler is $\Delta t \cdot f(x(t))$, while it is

$$\Delta t\left(k_1 + 2k_2 + 2k_3 + k_4\right)/6 \tag{2.44}$$

in the fourth order Runge–Kutta. The one step change in the Euler $\Delta t \cdot f(x(t))$ is determined by a single sample of the vector field at the point $x(t)$, while (2.44) is determined by four samples of the vector field evaluated at the current point $x(t)$ and the other three points $x(t) + \Delta t k_1/2$, $x(t) + \Delta t k_2/2$, and $x(t) + \Delta t k_3$ all of which are close to the point $x(t)$ for a small Δt. This one step movement procedure is summarized in Fig. 2.18. Intuitively, it is obvious that the fourth order

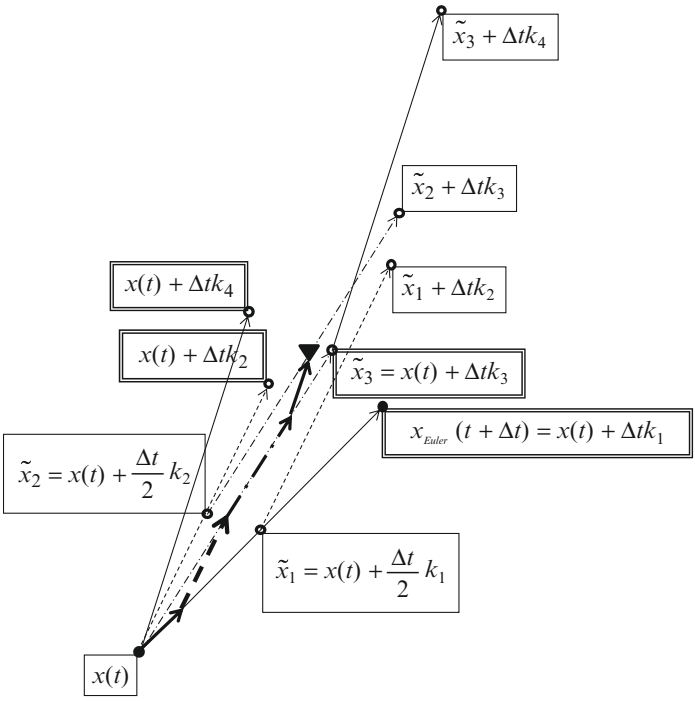


Fig. 2.18 Geometric representation of the fourth-order Runge–Kutta method. The *close circle* is an approximated state point $x(t + \Delta t)$ that is calculated by the forward Euler method from the state point $x(t)$. The *inverted-close triangle* is an approximated state point $x(t + \Delta t)$ obtained by the fourth-order Runge–Kutta method

Runge–Kutta gives better approximation because the one step movement is determined by examining structure of the vector field around the current state point $x(t)$ more in detail by taking a weighted average of those vector fields.

IDE Modeling: Periodically Forced FitzHugh–Nagumo (BVP) Model: Search ModelDB by "BVP" to Find Periodically_Stimulated_BVP_Model.isml

$$\frac{dv}{dt} = c\left(v - \frac{v^3}{3} - w + I_{dc} + I_{ext}(t)\right)$$
$$\frac{dw}{dt} = \frac{1}{c}(v - bw + a) \tag{2.45}$$

where $a = 0.7$, $b = 0.8$, and $c = 3.0$. I_{dc} and I_{ext} are the externally applied current with I_{dc} as the direct current component and $I_{ext}(t)$ as the time-dependent component. This is close to an original version of the FHN model (Nomura et al. 1994; Yoshino et al. 1999) but qualitatively the same as (2.36). Here we examine

excitable and oscillatory dynamics of the model for different values of the direct current I_{dc} as well as responses of the model to periodic current stimulations delivered as $I_{ext}(t)$. Figure 2.19 shows action potentials (thin curve) of the BVP model with two different values of I_{dc} in response to a sequence of periodic current pulse stimulations $I_{ext}(t)$ (thick curve) with the period T, the height A, and its width 0.05. The solutions are obtained by integrated with the forward Euler method with the time step 0.0005. In the upper panel, we set $I_{dc} = 0.1$ for which the model behaves as an excitable membrane showing a quiescent (equilibrium or resting) potential when no pulse train is applied for the first 100 ms, and then the model responds in a 3:1 *phase-locked entrainment* to the periodic stimulations ($T = 9.0$ ms and $A = 5.0$) by generating action potentials. In the middle, $I_{dc} = 0.1$ is used as in the upper panel showing a quiescent state for the first 100 ms. Then the model responds irregular-chaotically to the periodic stimulations ($T = 9.0$ ms and $A = 3.1395$). In the lower panel, we set $I_{dc} = 0.347$ for which the model behaves as an oscillatory membrane showing a self-sustained periodic action potentials when no pulse train is applied for the first 100 ms. This solution is a stable *limit cycle*, and it is often consider as a model of repetitive oscillations in *pacemaker cells*. After the onset of the pulse stimulations at 100 ms, the oscillator model responds in a 4:3 phase-locked entrainment to the periodic stimulations ($T = 8.0$ ms and $A = 5.0$). These dynamics can be typically observed in many nonlinear dynamical systems including biological and physiological systems. See Segundo et al. (1991) for a reference of neurophysiological observations associated with the nonlinear dynamics described in this example and thorough analyses of the experimental data. For a model-based analysis related to this example, see Doi and Sato (1995), Nomura et al. (1994), and Yoshino et al. (1999).

2.6 Examples from Cardiac Muscle Cell Models

The heart is one of the most important organs for animals and human. It is composed of cardiac muscle cells. Coordinated contractions of those cells generate heart beats and contractions of the whole heart, allowing blood to circulate in the body. Each contraction of a cardiac cell is controlled and regulated by its cellular excitation. In particular, calcium ions influx through the calcium channel and calcium ions released from calcium stores within a cell induce conformational changes in myofiber proteins, leading to the muscle contraction.

Mechanisms of action potential generation in cardiac cells are basically similar to those in squid axons. Thus, they have been modeled based on the Hodgkin–Huxley formulation and modifications of it. However, cardiac cells, as well as other excitable cells than the squid axons, behave differently if we look at details to some degree. This is natural because they might be responsible for much more complicated physiological roles of life and death than the squid axon. Variety of ion channels and cytoplasmic organella contribute to the action potential generation, muscle contraction, and regulation of them. Understanding the mechanisms is of importance clinically and pharmaceutically because drug-induced sudden cardiac

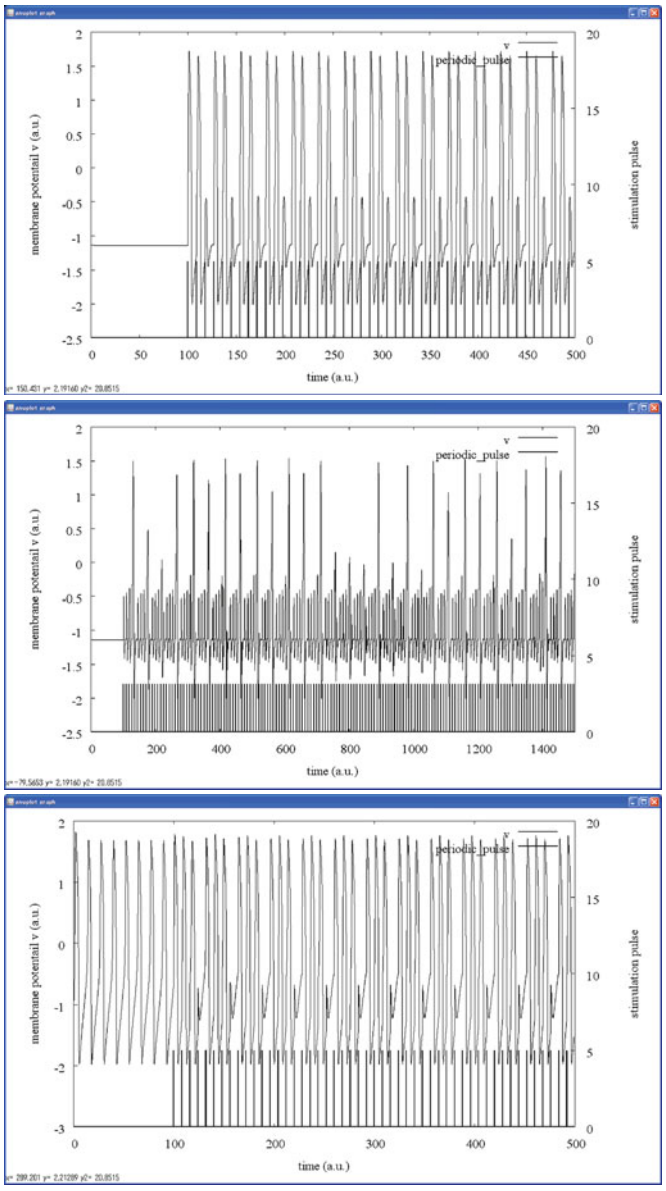


Fig. 2.19 Action potential (*thin curve*) of the BVP model with two different values of I_{dc} in response to a sequence periodic current pulse stimulations $I_{ext}(t)$ (*thick curve*) with the period T, the height A, and the width $w = 0.05$. The application of $I_{ext}(t)$ starts at $t = 100$. Solutions are obtained by the forward Euler method with the time step 0.0005. *Upper*: $I_{dc} = 0.1$ for which the model behaves as an excitable membrane showing a quiescent (resting) potential for the first 100 ms, and then responds in a 3:1 phase-locked entrainment to the periodic stimulations ($T = 9.0$ ms and $A = 5.0$). *Middle*: $I_{dc} = 0.1$ as in the upper for the first 100 ms, and then responds irregular-chaotically to the periodic stimulations ($T = 9.0$ ms and $A = 3.1395$). *Lower*: $I_{dc} = 0.347$ for which the model behaves as an oscillatory membrane (a limit cycle oscillator) showing a self-sustained periodic action potentials for the first 100 ms, and then it responds in a 4:3 phase-locked entrainment to the periodic stimulations ($T = 8.0$ ms and $A = 5.0$)

death and ventricular arrhythmia have arisen as serious public health concerns, in which these arrhythmia could result in withdrawal of non-cardiac drugs. Common drug-induced arrhythmia are due to molecular interaction between chemical compounds of drugs and ion channels (Roden 2004; Sanguinettia and Mitchesonb 2005). Here we briefly look at electrophysiological modeling of cardiac cells through several IDE examples.

A fast inward current of sodium channels is responsible for an onset of cardiac action potential in single cells as in the squid axon. Several kinds of outward potassium currents are also involved, but the time scale of their activations are slower than the axon. Moreover, slow inward currents of calcium channels play important roles, which makes, together with the slow potassium currents, duration of the action potential longer than those of neuronal action potentials. This contributes to stable conduction or propagation of action potentials through a cardiac tissue. The excitation conduction (see next chapter) is a key mechanism of the coordinated muscle contraction starting from a pacemaker site (sino-atrial node) of the heart located at the atrium and then to atrio-ventricular node and the ventricle muscles. The pacemaker cells spontaneously and rhythmically generate action potentials for pacemaking the heart beat.

IDE Modeling: Beeler Reuter Cardiac Ventricular Cell Model: Search ModelDB by "Reuter" to Find Beeler_Reuter_1977_Model.isml

$$\begin{aligned}
\frac{dV_m}{dt} &= -\frac{1}{C_m}\left(i_{K1} + i_{x1} + i_{Na} + i_s - i_{external}\right) \\
i_{Na} &= \left(\bar{g}_{Na} m^3 hj + g_{NaC}\right)\left(V_m - E_{Na}\right) \\
i_s &= \bar{g}_s df\left(V_m - E_s\right) \\
\frac{d[Ca^{2+}]_i}{dt} &= -10^{-7} i_s + 0.07\left(10^{-7} - [Ca^{2+}]_i\right) \\
E_s &= -82.3 - 13.0287 \ln[Ca^{2+}]_i
\end{aligned} \tag{2.46}$$

where V_m represents the membrane potential, i_{K1} the time-independent potassium outward current, i_{x1} the time-activated outward current, i_{Na} the fast inward sodium current, i_{Ca} the calcium current, $[Ca]_i$ the intracellular calcium concentration, and i_s the slow inward current carried mainly by Ca^{2+}. m, h, j, d, and f are gating variables among other gating variables that are not shown in (2.46). This is a rough description of the Beeler Reuter (BR) model, which is a Hodgkin–Huxley like formulation of a cardiac ventricular cell (Beeler and Reuter 1977). Here we examine its dynamics. This model or several more pioneering models (Noble 1962) triggered a long history up to the present date for understanding cellular excitations and ion channels based on reproduction of electrophysiological observations using mathematical models. Figure 2.20-upper shows a snapshot of the *insilico*IDE canvas

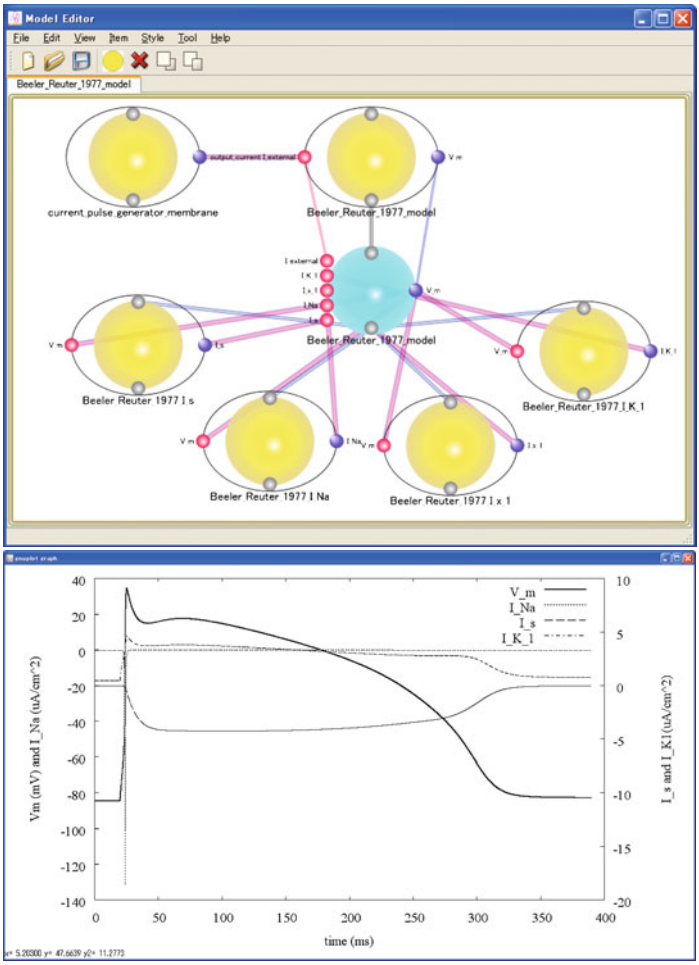


Fig. 2.20 *Upper*: A snapshot of insilicoIDE for the Beeler Reuter (BR) model of a cardiac ventricular cell with a single pulsatile current injection. *Lower*: A response of the model to the single current pulse stimulation. *Thick-solid* represents the membrane potential V_m, *dotted* the sodium current i_{Na}, *dashed* the slow inward current primary carried by Ca^{2+} ions i_s, *dash-dotted* the potassium current i_{K1}

on which a set of modules representing the model is displayed. The action potential waveform is shown in Fig. 2.20-lower with i_{Na}, i_s, and i_{K1}. As in Fig. 2.16-upper, several modules at lower layer of the model, up to the ion current level, are expanded and shown. One can compare that the HH model has three ion current modules in Fig. 2.16 while the BR model has four ion current modules. Despite of the fact that the BR model was constructed only after a decade from the Hodgkin–Huxley with a small modification of the HH, we have already started to feel a hesitation to write down a whole set of equations for the BR model, representing our situation nowadays of how deeply we are struggling against the variety and complexity of the

real world modeling. Nevertheless, the whole set of the equations of the BR model is fully described here. Let us emphasize that the description of the BR model here is automatically generated by the *insilico*IDE software which exports the BR model in ISML format into a LaTeX source file to be just pasted in this textbook as follows. The BR model is expressed by 46 equations including the equations for defining parameter values.

I Beeler_Reuter_1977_Model

This is a capsule module. This model represents the Beeler–Reuter model [Beeler GW, Reuter H (1977) Reconstruction of the action potential of ventricular myocardial fibres. J Physiol 268(1):177–210].

I.1 Beeler_Reuter_1977_I_x_1

This module represents the time-activated outward current model used in the Beeler–Reuter model (Beeler and Reuter 1977). See Sect. V for details.

I.2 Beeler_Reuter_1977_I_Na

This module represents the initial fast inward current model used in the Beeler–Reuter model (Beeler and Reuter 1977). See Sect. III for details.

I.3 Beeler_Reuter_1977_I_K_1

This module represents the time-independent potassium outward current model used in the Beeler–Reuter model (Beeler and Reuter 1977). See Sect. II for details.

I.4 Beeler_Reuter_1977_Model

This model represents the Beeler–Reuter model (Beeler and Reuter 1977).

I.4.1 Physical Quantities

⋆ $shape$ **: morphology**
Definition :
The morphology is assigned to this physical quantity
⋆ V_m **: state**
The membrane potential taken as inside potential minus outside potential
Definition :

$$\frac{d}{dt} V_m = \frac{(-((I_K_1 + I_x_1 + I_Na + I_s) - I_external))}{C_m} \tag{2.47}$$

with the initial condition

$$V_m = -84.5737 \tag{2.48}$$

This value is used in

Module "Beeler_Reuter_1977_model" (Sect. I), physical-quantity ""
Module "I_s" (Sect. IV.2), physical-quantity "V_m"
Module "d_gate" (Sect. IV.5), physical-quantity "V_m"
Module "f_gate" (Sect. IV.1), physical-quantity "V_m"
Module "I_Na" (Sect. III.1), physical-quantity "V_m"
Module "m_gate" (Sect. III.3), physical-quantity "V_m"
Module "h_gate" (Sect. III.2), physical-quantity "V_m"
Module "j_gate" (Sect. III.4), physical-quantity "V_m"
Module "I_x_1_bar" (Sect. V.2), physical-quantity "V_m"
Module "x_1_gate" (Sect. V.1), physical-quantity "V_m"
Module "I_K_1" (Sect. II.1), physical-quantity "V_m"

⋆ C_m **: static-parameter**
The membrane capacity per unit area
Definition :

$$C_m = 1 \tag{2.49}$$

⋆ $I_external$ **: variable-parameter**
This port inputs I_extarnal (current stimulus).
Definition :
The value is given by other module through edge and port
Origin of the value is the Module "current_pulse_generator_membrane" (Sect. VI.1), physical-quantity "*current_in_micro_ampere_per_centi_meter2*"

⋆ I_K_1 **: variable-parameter**
This port inputs I_K_1 (the time-independent potassium outward current).
Definition :
The value is given by other module through edge and port
Origin of the value is the Module "I_K_1" (Sect. II.1), physical-quantity "I_K_1"

⋆ I_x_1 **: variable-parameter**
This port inputs I_x_1 (the time-activated outward current).
Definition :
The value is given by other module through edge and port
Origin of the value is the Module "I_x_1" (Sect. V.3), physical-quantity "I_x_1"

⋆ I_Na **: variable-parameter**
This port inputs I_Na (the initial fast inward current carried primarily by sodium).
Definition :
The value is given by other module through edge and port
Origin of the value is the Module "I_Na" (Sect. III.1), physical-quantity "I_Na"

⋆ I_s **: variable-parameter**
This port inputs I_s (the secondary or slow inward current primarily carried by calcium ions).
Definition :
The value is given by other module through edge and port
Origin of the value is the Module "I_s" (Sect. IV.2), physical-quantity "I_s"

I.5 Beeler_Reuter_1977_I_s

This module represents the secondary or slow inward current model used in the Beeler–Reuter model (Beeler and Reuter 1977). See Sect. IV for details.

II Beeler_Reuter_1977_I_K_1

This is a capsule module. This module represents the time-independent potassium outward current model used in the Beeler–Reuter model (Beeler and Reuter 1977).

II.1 I_K_1

The time-independent potassium outward current

II.1.1 Physical Quantities

⋆ *shape* **: morphology**
Definition :
The morphology is assigned to this physical quantity

⋆ *I_K_1* **: variable-parameter**
The time-independent potassium outward current
Definition :

$$I_K_1 = 0.35 \left(\frac{4 \ (\exp(0.04 \ (V_m + 85)) - 1)}{(\exp(0.08 \ (V_m + 53)) + \exp(0.04 \ (V_m + 53)))} + \frac{0.2 \ (V_m + 23)}{(1 - \exp(-0.04 \ (V_m + 23)))} \right) \tag{2.50}$$

This value is used in
Module "Beeler_Reuter_1977_model" (Sect. I.4), physical-quantity "*I_K_1*"

⋆ *V_m* **: variable-parameter**
This port inputs V_m (the membrane potential taken as inside potential minus outside potential).
Definition :
The value is given by other module through edge and port
Origin of the value is the Module "Beeler_Reuter_1977_model" (Sect. I.4), physical-quantity "*V_m*"

III Beeler_Reuter_1977_I_Na

This is a capsule module. This module represents the initial fast inward current model used in the Beeler–Reuter model (Beeler and Reuter 1977).

III.1 I_Na

The initial fast inward current carried primarily by sodium

III.1.1 Physical Quantities

⋆ *shape* **: morphology**
Definition :
The morphology is assigned to this physical quantity

⋆ *g_Na_bar* **: static-parameter**
The fully activated sodium conductance
Definition :

$$g_Na_bar = 4 \tag{2.51}$$

⋆ *g_NaC* **: static-parameter**
The background sodium conductance
Definition :

$$g_NaC = 0.003 \tag{2.52}$$

⋆ *E_Na* **: static-parameter**
The reversal potential of Na
Definition :

$$E_Na = 50 \tag{2.53}$$

⋆ *I_Na* **: variable-parameter**
The initial fast inward current carried primarily by sodium
Definition :

$$I_Na = (g_Na_bar\ m\ m\ m\ h\ j + g_NaC)\ \ (V_m - E_Na) \tag{2.54}$$

This value is used in
Module "Beeler_Reuter_1977_model" (Sect. I.4), physical-quantity "*I_Na*"

⋆ *V_m* **: variable-parameter**
This port inputs V_m (the membrane potential taken as inside potential minus outside potential).
Definition :
The value is given by other module through edge and port
Origin of the value is the Module "Beeler_Reuter_1977_model" (Sect. I.4), physical-quantity "*V_m*"

⋆ *m* **: variable-parameter**
This port inputs m (the proportion of activation gate of I_Na).
Definition :
The value is given by other module through edge and port
Origin of the value is the Module "m_gate" (Sect. III.3), physical-quantity "*m*"

⋆ *h* **: variable-parameter**
This port inputs h (the proportion of first inactivation gate of I_Na).
Definition :
The value is given by other module through edge and port
Origin of the value is the Module "h_gate" (Sect. III.2), physical-quantity "*h*"

⋆ *j* **: variable-parameter**
This port inputs j (the proportion of slow inactivation gate of I_Na).
Definition :
The value is given by other module through edge and port
Origin of the value is the Module "j_gate" (Sect. III.4), physical-quantity "*j*"

III.2 h_gate

The proportion of first inactivation gate of I_Na

III.2.1 Physical Quantities

⋆ *shape* **: morphology**
Definition :
The morphology is assigned to this physical quantity

⋆ h **: state**
The proportion of first inactivation gate of I_Na
Definition :

$$\frac{d}{dt}h = (alpha_h\ (1-h) - beta_h\ h) \tag{2.55}$$

with the initial condition

$$h = 0.987721 \tag{2.56}$$

This value is used in
Module "I_Na" (Sect. III.1), physical-quantity "h"

⋆ *alpha_h* **: variable-parameter**
Opening rate constants of h-gate
Definition :

$$alpha_h = \frac{(0.126\ \exp(-0.25\ (V_m + 77)) + 0\ (V_m + 0))}{(\exp(0\ (V_m + 77)) + 0)} \tag{2.57}$$

⋆ *beta_h* **: variable-parameter**
Closing rate constants of h-gate
Definition :

$$beta_h = \frac{(1.7\ \exp(0\ (V_m + 22.5)) + 0\ (V_m + 0))}{(\exp(-0.082\ (V_m + 22.5)) + 1)} \tag{2.58}$$

⋆ V_m **: variable-parameter**
This port inputs V_m (the membrane potential taken as inside potential minus outside potential).
Definition :
The value is given by other module through edge and port
Origin of the value is the Module "Beeler_Reuter_1977_model" (Sect. I.4), physical-quantity "V_m"

III.3 m_gate

The proportion of activation gate of I_Na

III.3.1 Physical Quantities

⋆ *shape* **: morphology**
Definition :
The morphology is assigned to this physical quantity

⋆ m **: state**
The proportion of activation gate of I_Na
Definition :

$$\frac{d}{dt}m = (alpha_m\ (1 - m) - beta_m\ m) \tag{2.59}$$

with the initial condition

$$m = 0.010982 \tag{2.60}$$

This value is used in
Module "I_Na" (Sect. III.1), physical-quantity "m"

⋆ $alpha_m$ **: variable-parameter**
Opening rate constants of m-gate
Definition :

$$alpha_m = \frac{(0\ \exp(0\ (V_m + 47)) - (V_m + 47))}{(\exp(-0.1\ (V_m + 47)) - 1)} \tag{2.61}$$

⋆ $beta_m$ **: variable-parameter**
Closing rate constants of m-gate
Definition :

$$beta_m = \frac{(40\ \exp(-0.056\ (V_m + 72)) + 0\ (V_m + 0))}{(\exp(0\ (V_m + 72)) + 0)} \tag{2.62}$$

⋆ V_m **: variable-parameter**
This port inputs V_m (the membrane potential taken as inside potential minus outside potential).
Definition :
The value is given by other module through edge and port
Origin of the value is the Module "Beeler_Reuter_1977_model" (Sect. I.4), physical-quantity "V_m"

III.4 j_gate

The proportion of slow inactivation gate of I_Na

III.4.1 Physical Quantities

⋆ $shape$ **: morphology**
Definition :
The morphology is assigned to this physical quantity

⋆ j **: state**
The proportion of slow inactivation gate of I_Na
Definition :

$$\frac{d}{dt}j = (alpha_j\ (1 - j) - beta_j\ j) \tag{2.63}$$

with the initial condition

$$j = 0.974838 \tag{2.64}$$

This value is used in
Module "I_Na" (Sect. III.1), physical-quantity "j"

⋆ *alpha_j* **: variable-parameter**
Opening rate constants of j-gate
Definition :

$$alpha_j = \frac{(0.055\ \exp(-0.25\ (V_m + 78)) + 0\ (V_m + 0))}{(\exp(-0.2\ (V_m + 78)) + 1)} \tag{2.65}$$

⋆ *beta_j* **: variable-parameter**
Closing rate constants of j- gate
Definition :

$$beta_j = \frac{(0.3\ \exp(0\ (V_m + 32)) + 0\ (V_m + 0))}{(\exp(-0.1\ (V_m + 32)) + 1)} \tag{2.66}$$

⋆ *V_m* **: variable-parameter**
This port inputs V_m (the membrane potential taken as inside potential minus outside potential).
Definition :
The value is given by other module through edge and port
Origin of the value is the Module "Beeler_Reuter_1977_model" (Sect. I.4), physical-quantity "*V_m*"

IV Beeler_Reuter_1977_I_s

This is a capsule module. This module represents the secondary or slow inward current model used in the Beeler–Reuter model (Beeler and Reuter 1977).

IV.1 f_gate

The proportion of inactivation gate of I_s

IV.1.1 Physical Quantities

⋆ *shape* **: morphology**
Definition :
The morphology is assigned to this physical quantity

⋆ f **: state**
The proportion of inactivation gate of I_s
Definition :

$$\frac{d}{dt} f = (alpha_f\ (1 - f) - beta_f\ f) \tag{2.67}$$

with the initial condition

$$f = 0.999981 \tag{2.68}$$

This value is used in
Module "I_s" (Sect. IV.2), physical-quantity "f"

⋆ *alpha_f* **: variable-parameter**
Opening rate constants of f-gate
Definition :

$$alpha_f = \frac{(0.012\ \exp(-0.008\ (V_m + 28)) + 0\ (V_m + 0))}{(\exp(0.15\ (V_m + 28)) + 1)} \tag{2.69}$$

⋆ *beta_f* **: variable-parameter**
Closing rate constants of f-gate
Definition :

$$beta_f = \frac{(0.0065\ \exp(-0.02\ (V_m + 30)) + 0\ (V_m + 0))}{(\exp(-0.2\ (V_m + 30)) + 1)} \tag{2.70}$$

⋆ *V_m* **: variable-parameter**
This port inputs V_m (the membrane potential taken as inside potential minus outside potential).
Definition :
The value is given by other module through edge and port
Origin of the value is the Module "Beeler_Reuter_1977_model" (Sect. I.4), physical-quantity "*V_m*"

IV.2 I_s

The secondary or slow inward current primarily carried by calcium ions

IV.2.1 Physical Quantities

⋆ *shape* **: morphology**
Definition :
The morphology is assigned to this physical quantity

⋆ *g_s_bar* **: static-parameter**
The fully activated conductance of slow inward ions
Definition :

$$g_s_bar = 0.09 \tag{2.71}$$

⋆ *I_s* **: variable-parameter**
The secondary or slow inward current primarily carried by calcium ions
Definition :

$$I_s = g_s_bar\ d\ f\ \ (V_m - E_s) \tag{2.72}$$

This value is used in
Module "Beeler_Reuter_1977_model" (Sect. I.4), physical-quantity "*I_s*"
Module "Ca_i" (Sect. IV.3), physical-quantity "*I_s*"

⋆ *V_m* **: variable-parameter**
This port inputs V_m (the membrane potential taken as inside potential minus outside potential).
Definition :
The value is given by other module through edge and port
Origin of the value is the Module "Beeler_Reuter_1977_model" (Sect. I.4), physical-quantity "*V_m*"

⋆ *E_s* **: variable-parameter**
This port inputs E_s (the reversal potential of slow inward ions).
Definition :
The value is given by other module through edge and port
Origin of the value is the Module "E_s" (Sect. IV.4), physical-quantity "*E_s*"

⋆ *d* **: variable-parameter**
This port inputs d (the proportion of activation gate of I_s).

Definition :
The value is given by other module through edge and port
Origin of the value is the Module "d_gate" (Sect. IV.5), physical-quantity "d"

⋆ f **: variable-parameter**
This port inputs f (the proportion of inactivation gate of I_s).
Definition :
The value is given by other module through edge and port
Origin of the value is the Module "f_gate" (Sect. IV.1), physical-quantity "f"

IV.3 Ca_i

The intracellular calcium concentration

IV.3.1 Physical Quantities

⋆ *shape* **: morphology**
Definition :
The morphology is assigned to this physical quantity

⋆ Ca_i **: state**
The intracellular calcium concentration
Definition :

$$\frac{d}{dt} Ca_i = (-0.0000001\ I_s + 0.07\ (0.0000001 - Ca_i)) \tag{2.73}$$

with the initial condition

$$Ca_i = 0.000000178201 \tag{2.74}$$

This value is used in
Module "E_s" (Sect. IV.4), physical-quantity "Ca_i"

⋆ I_s **: variable-parameter**
This port inputs I_s (the secondary or slow inward current primarily carried by calcium ions).
Definition :
The value is given by other module through edge and port
Origin of the value is the Module "I_s" (Sect. IV.2), physical-quantity "I_s"

IV.4 E_s

The reversal potential of slow inward ions

IV.4.1 Physical Quantities

⋆ *shape* **: morphology**
Definition :
The morphology is assigned to this physical quantity

⋆ E_s **: variable-parameter**
The reversal potential of slow inward ions
Definition :

$$E_s = (-82.3 - 13.0287\ \ln(Ca_i)) \tag{2.75}$$

This value is used in
Module "I_s" (Sect. IV.2), physical-quantity "E_s"

⋆ Ca_i **: variable-parameter**
This port inputs Ca_i (the intracellular calcium concentration).
Definition :
The value is given by other module through edge and port
Origin of the value is the Module "Ca_i" (Sect. IV.3), physical-quantity "Ca_i"

IV.5 d_gate

The proportion of activation gate of I_s

IV.5.1 Physical Quantities

⋆ *shape* **: morphology**
Definition :
The morphology is assigned to this physical quantity

⋆ d **: state**
The proportion of activation gate of I_s
Definition :

$$\frac{d}{dt}d = (alpha_d\ \ (1 - d) - beta_d\ d) \tag{2.76}$$

with the initial condition

$$d = 0.00297072 \tag{2.77}$$

This value is used in
Module "I_s" (Sect. IV.2), physical-quantity "d"

⋆ $alpha_d$ **: variable-parameter**
Opening rate constants of d-gate
Definition :

$$alpha_d = \frac{(0.095\ \exp(-0.01\ \ (V_m - 5)) + 0\ \ (V_m + 0))}{(\exp(-0.072\ \ (V_m - 5)) + 1)} \tag{2.78}$$

⋆ $beta_d$ **: variable-parameter**
Closing rate constants of d-gate
Definition :

$$beta_d = \frac{(0.07\ \exp(-0.017\ \ (V_m + 44)) + 0\ \ (V_m + 0))}{(\exp(0.05\ \ (V_m + 44)) + 1)} \tag{2.79}$$

⋆ V_m **: variable-parameter**
This port inputs V_m (the membrane potential taken as inside potential minus outside potential).
Definition :
The value is given by other module through edge and port
Origin of the value is the Module "Beeler_Reuter_1977_model" (Sect. I.4), physical-quantity "V_m"

V Beeler_Reuter_1977_I_x_1

This is a capsule module. This module represents the time-activated outward current model used in the Beeler–Reuter model (Beeler and Reuter 1977).

V.1 x_1_gate

The proportion of activation gate of I_x_1

V.1.1 Physical Quantities

⋆ *shape* **: morphology**
Definition :
The morphology is assigned to this physical quantity

⋆ x_1 **: state**
The proportion of activation gate of I_x_1
Definition :

$$\frac{d}{dt}x_1 = (alpha_x_1\ \ (1 - x_1) - beta_x_1\ x_1) \tag{2.80}$$

with the initial condition

$$x_1 = 0.00562868 \tag{2.81}$$

This value is used in
Module "I_x_1" (Sect. V.3), physical-quantity "x_1"

⋆ $alpha_x_1$ **: variable-parameter**
Opening rate constants of x_1-gate
Definition :

$$alpha_x_1 = \frac{(0.0005\ \exp(0.083\ \ (V_m + 50)) + 0\ \ (V_m + 0))}{(\exp(0.057\ \ (V_m + 50)) + 1)} \tag{2.82}$$

⋆ $beta_x_1$ **: variable-parameter**
Closing rate constants of x_1-gate
Definition :

$$beta_x_1 = \frac{(0.0013\ \exp(-0.06\ \ (V_m + 20)) + 0\ \ (V_m + 0))}{(\exp(-0.04\ \ (V_m + 20)) + 1)} \tag{2.83}$$

⋆ V_m **: variable-parameter**
This port inputs V_m (the membrane potential taken as inside potential minus outside potential).
Definition :
The value is given by other module through edge and port
Origin of the value is the Module "Beeler_Reuter_1977_model" (Sect. I.4), physical-quantity "V_m"

V.2 I_x_1_bar

The maximum time-activated outward current

V.2.1 Physical Quantities

⋆ *shape* **: morphology**
Definition :
The morphology is assigned to this physical quantity

⋆ *I_x_1_bar* **: variable-parameter**
The maximum time-activated outward current
Definition :

$$I_x_1_bar = \frac{0.8\ (\exp(0.04\ (V_m + 77)) - 1)}{\exp(0.04\ (V_m + 35))} \tag{2.84}$$

This value is used in
Module "I_x_1" (Sect. V.3), physical-quantity "*I_x_1_bar*"

⋆ *V_m* **: variable-parameter**
This port inputs V_m (the membrane potential taken as inside potential minus outside potential).
Definition :
The value is given by other module through edge and port
Origin of the value is the Module "Beeler_Reuter_1977_model" (Sect. I.4), physical-quantity "*V_m*"

V.3 I_x_1

The time-activated outward current

V.3.1 Physical Quantities

⋆ *shape* **: morphology**
Definition :
The morphology is assigned to this physical quantity

⋆ *I_x_1* **: variable-parameter**
The time-activated outward current
Definition :

$$I_x_1 = I_x_1_bar\ x_1 \tag{2.85}$$

This value is used in
Module "Beeler_Reuter_1977_model" (Sect. I.4), physical-quantity "*I_x_1*"

⋆ *I_x_1_bar* **: variable-parameter**
This port inputs I_x_1_bar (the maximum time-activated outward current).
Definition :
The value is given by other module through edge and port
Origin of the value is the Module "I_x_1_bar" (Sect. V.2), physical-quantity "*I_x_1_bar*"

⋆ *x_1* **: variable-parameter**
This port inputs x_1(the proportion of activation gate of I_x_1).
Definition :
The value is given by other module through edge and port
Origin of the value is the Module "x_1_gate" (Sect. V.1), physical-quantity "*x_1*"

VI Current_pulse_generator_membrane

This is a capsule module. current pulse generator module

VI.1 Current_pulse_generator_membrane

Current pulse generator module

VI.1.1 Physical Quantities

⋆ *shape* **: morphology**
Definition :
The morphology is assigned to this physical quantity

⋆ *pulse_onset_time* **: static-parameter**
The time instance when the pulse takes place.
Definition :

$$pulse_onset_time = 20 \tag{2.86}$$

⋆ *pulse_width* **: static-parameter**
The pulse width in milli-second.
Definition :

$$pulse_width = 5 \tag{2.87}$$

⋆ *pulse_height* **: static-parameter**
The height of the pulse.
Definition :

$$pulse_height = 10 \tag{2.88}$$

⋆ *initial_ampere* **: static-parameter**
The current in micro-ampere per centi-meter2 before and after the pulse.
Definition :

$$initial_ampere = 0 \tag{2.89}$$

⋆ *current_in_micro_ampere_per_centi_meter2* **: variable-parameter**
The current value changes from an initial value (parameter: initial_ampere) to another value (parameter: pulse_height) at a given onset time (parameter: pulse_onset_time) and after the pulse_width return to the initial value.
Definition :
When the condition

$$(time \geq pulse_onset_time \text{ and } time < (pulse_onset_time + pulse_width)) \tag{2.90}$$

is satisfied, then

$$current_in_micro_ampere_per_centi_meter2 = (pulse_height + initial_ampere) \tag{2.91}$$

otherwise

$$current_in_micro_ampere_per_centi_meter2 = initial_ampere \tag{2.92}$$

This value is used in

Module "Beeler_Reuter_1977_model" (Sect. I.4), physical-quantity "*I_external*"

VII Capsule_of_Beeler_Reuter_1977_model

This is a capsule module.

VII.1 Current_pulse_generator_membrane

Current pulse generator module. See Sect. VI for details.

VII.2 Beeler_Reuter_1977_Model

This model represents the Beeler–Reuter model (Beeler and Reuter 1977). See Sect. I for details.

As briefly mentioned above, the calcium ions play dominant roles in the muscle contraction. The cytoplasmic Ca^{2+} concentration in cardiac myocytes is kept extremely low at around $0.1\ \mu M$. An increase of intracellular Ca^{2+} concentration is usually caused by Ca^{2+} influx from the extracellular space and/or Ca^{2+} release from intracellular organelles. Ca^{2+} provides a coupling between electrical excitation and contraction of the cell. The L-type calcium channel on the sarcolemma opens in response to membrane depolarization, allowing Ca^{2+} influx into the dyadic subspace, the narrow space in the cytoplasm between the cell surface and sarcoplasmic reticulum (SR) membranes. When Ca^{2+} influx from the L-type calcium channel diffuses within the dyadic subspace and reaches ryanodine receptors on the SR surface, they trigger Ca^{2+} release from the SR via these receptors, causing further elevation of the cytoplasmic Ca^{2+} concentration. This is known as the *calcium induced calcium release* (CICR) (Fabiato 1985), leading to Ca^{2+} binding to the protein called troponin C for muscle fiber contraction. See Fig. 2.21 for a cartoon of a typical cardiac cell membrane.

IDE Modeling: Faber–Rudy Cardiac Ventricular Cell Model: Search ModelDB by "Rudy" to Find Faber_Rudy_2007_Model.isml

$$C_m \frac{dV_m}{dt} = -I_{FaberRudy} + I_{ext} \tag{2.93}$$

Faber–Rudy (FR) model (Faber et al. 2007) is one of the most detailed model of a single cardiac ventricular cell. We automatically exported the ISML model of the FR model into a LaTeXsource file as we performed for the BR model using the

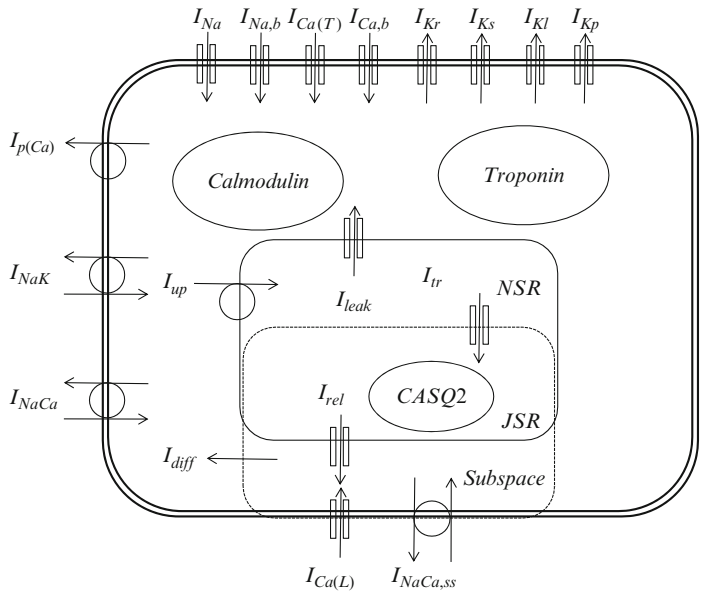


Fig. 2.21 Biophysically detailed model of cardiac ventricular cell membrane

*insilico*IDE, and confirmed that the FR model is described by 333 equations including the ones for defining values of parameters. One could claim that this number (333) is still within a human tractable range for a computational biologist, and it might be true. However, it might also be true that it is not easy task to write every of those equations by hands and to find typos that may be included in the manually produced code. Figure 2.21 illustrates most of the cellular entities included in the FR model. One can see 12 types of ion channels, within which nine are on the plasma membrane and three on the cytoplasma membranes of the intracellular organella, such as the sarcoplasmic reticulum (SR) that stores calcium ions necessary for the muscle contraction. In the FR model, the SR is further divided into two spaces, namely JSR (Junctional SR) and NSR (Network SR). A small space between the cellular membrane and the SR is referred to as the *subspace* or the *dyadic space*. These spaces are illustrated in Fig. 2.21 as square-like boxes located in the cytoplasmic space. Although the model does not explicitly describe the cellular geometry such as the shapes and locations of the SR, the model describes the ion concentration of each of these spaces, such as $[Ca^{2+}]_i$ for the cytoplasmic space and $[Ca^{2+}]_{ss}$ for the dyadic subspace which is determined by

$$\frac{d[Ca^{2+}]_{ss}}{dt} = -\beta_{ss}\left((I_{Ca(L)} - 2I_{NaCa,ss})\frac{A_{cap}}{V_{ss}z_{ca}F} - I_{rel}\frac{V_{JSR}}{V_{ss}} + I_{diff}\right) \tag{2.94}$$

where $I_{Ca(L)}$, $I_{NaCa,ss}$, I_{rel}, and I_{diff} represent, respectively, the currents of the L-type calcium channel, the Na^+–Ca^{2+} exchanger in the subspace, the calcium

release from the SR into the dyadic subspace inducing the CICR, and the calcium diffusion between the dyadic subspace and the cytoplasmic space. The calcium diffusion is modeled as

$$I_{diff} = \frac{[Ca^{2+}]_{ss} - [Ca^{2+}]_i}{\tau_{diff}} \tag{2.95}$$

as illustrated in Fig. 2.21. This is a simplification of diffusive transportation of Ca^{2+} between these spaces in the ordinary differential equation framework. The model also includes four active ion–ion exchangers (pumps) which are shown as circles on the membranes with one or two arrows representing flows of pumped ions. Figure 2.22-upper shows a snapshot of *insilico*IDE for the FR model with current pulse stimulation generator on the top-left of the panel, while on the right, a set of modules representing the model is displayed where modules at lower layers of the model are expanded still up to the ion current level as in Figs. 2.16 and 2.20. In contrast with Figs. 2.16 and 2.20, the FR model has a lot of lower layer modules because of its complexity in terms of types of ion channels and pumps as well as the intracellular organella. We will look at the FR model in more detail below, in particular, how the L-type calcium channel is modeled. In the lower panels of Fig. 2.22, a response of the FR model to a current pulse stimulation is depicted. The reader is recommended to download the FR model for execution to compare the action potential and the ion currents with those of the BR model in Fig. 2.20.

2.7 Variety of Complex Dynamics of Ion Channels

A number of cellular ion channels have been identified (Hille 2001). They can be classified into several types, or hundred of types if we consider in detail. The classification is made by their gating property and the types of ion that can selectively pass through the channel. Voltage-gated ion channels open or close depending on the voltage across the plasma membrane. Such channel proteins change their structural conformation depending on the membrane potential. In the Hodgkin–Huxley modeling, this voltage-gated property is modeled by the voltage-dependent rate functions $\alpha(V)$ and $\beta(V)$ for each type of the gate. Ligand-gated ion channels open or close depending on binding of ligands to the channel. The term "ligand" is a Latin word meaning "to bind," and in our context, protein molecules that bind to channels or receptors are ligands. Some ligand-gated channels open or close when a ligand outside the cell (extracellular space) binds to the channel, while others when a ligand inside the cell (intracellular space) binds to the channel. Ligand binding causes changes in structural conformation of the channel protein, leading to the opening or closing of the channel. Another type of channels open or close depending on second messengers which are molecules relaying signals from receptors on the cell surface to target molecules inside the cell. This is similar to the action of ligands inside the cell. Ions such as Ca^{2+} could also be considered as second messengers. For example, the L-type calcium channel that we used in the Faber–Rudy model is a

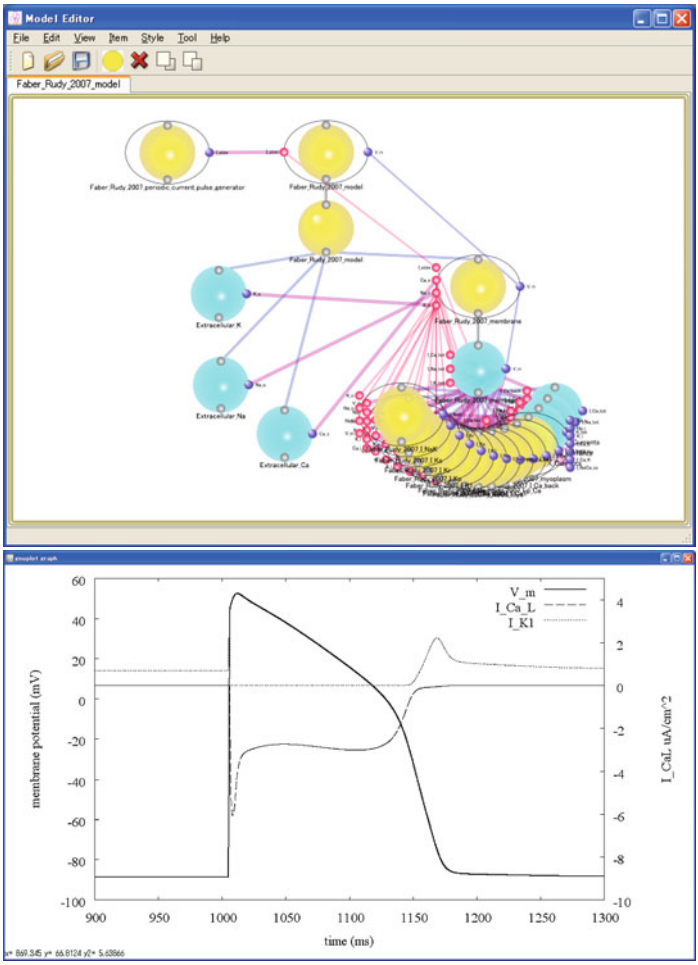


Fig. 2.22 *Upper*: A snapshot of insilicoIDE for the Faber–Rudy model of a cardiac ventricular cell with current pulse stimulations. *Lower*: A response of the model to a current pulse stimulation. *Thick-solid curve* represents the membrane potential V_m, the *dashed* the L-type Ca^{2+} current, and the *dotted* the potassium I_{K1} current. Compare with the BR model in Fig. 2.20

voltage-gated channel, but it is also inactivated by calcium ions. More specifically, Ca^{2+} ions by the influx of L-type calcium channel bind to a type of protein called calmodulin to form a calmodulin–Ca^{2+} complex which binds to the L-type calcium channel and inactivates the channel in a self-feedback manner.

Not all types of channel with such complexity can be modeled by the Hodgkin–Huxley-like gating formulation. This is partially because the HH formulation assumes independence of open–close kinetics of distinguished gates. Moreover, the HH-based gates were introduced hypothetically just to account for channel current dynamics, and they have less correspondence to structures of proteins as real

physical entities. A relatively simple example suggesting a limitation of the HH-based gating is the inactivation of the Na^+ channel if it is examined in detail. It has been shown that the inactivation of the sodium channel occurs with a larger probability when the channel is open (Armstrong and Bezanilla 1977). This means that the inactivation depends on the states of activation. In terms of the HH gates, this corresponds to a case where closing probability of the h-gate of a single channel depends on if the m-gates of the channel are in their open states or not. This is out of range of the HH gating assumption of stochastic independence among three m-gates and one h-gate, which allows us to multiply three ms and h in obtaining the conductance of the sodium channel. A class of models called *Markov models* can represent more accurately the dependence of a given transition on the occupancy of different states of the channel. See a review by Rudy and Silva (2006) for thorough description on this issue.

Here we only look at several simple examples to compare HH-based gate models and Markov models. Let us consider a simple hypothetical channel with a single open (O) and a single closed (C) state (Fig. 2.23a). The Markov model for this channel is described by the following ODEs.

$$\frac{dC}{dt} = -\alpha C + \beta O, \tag{2.96}$$

$$\frac{dO}{dt} = \alpha C - \beta O, \tag{2.97}$$

where C and O represent the probabilities, respectively, that the state of the channel is in the closed and the open, α and β the transition rates between these two states with their units 1/ms. α and β may be voltage-dependent if the channel is a voltage-gated. In the Markov model, the states C and O represent two different structural conformations of the channel protein. Since the state of the channel is in either closed or open, $C + O = 1$ always holds. For this simple case, we have a HH-based gate model representing exactly the same channel dynamics. Indeed, if we hypothesize a single gate, say m, the probability O can be represented as m, and the probability C as $1 - m$. Then, (2.97) is rewritten as

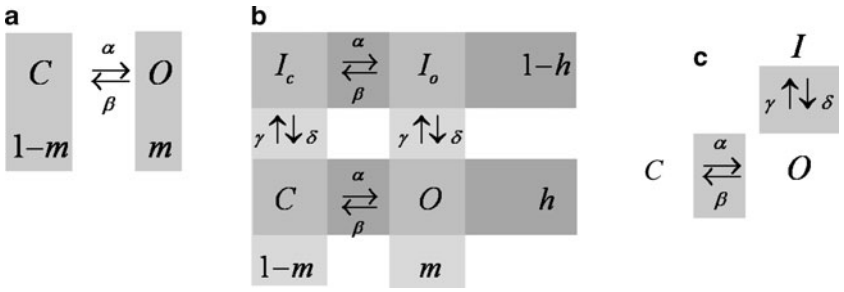


Fig. 2.23 Modeling of ion channel kinetics based on HH-type and Markov-type formulations

$$\frac{d(1-m)}{dt} = -\alpha(1-m) + \beta m,$$

$$\frac{dm}{dt} = \alpha(1-m) - \beta m,$$

in which we have two identical equations. This simple model can be represented by both HH-based gate model and Markov model because there is no state-dependent transition.

Let us consider one more simple example that can also be represented both by HH-based gate model and by Markov model (Fig. 2.23b). We start by a Markov model by assuming four different conformations of the channel. They are closed C, open O, and two inactivated states I_C and I_O. When a channel is in an inactivated state, no ions can flow through the channel, but it is distinguished from the closed state. In this example, I_C is the inactivated state of the closed state, which means that the conformation of I_C is established by a structural change from the closed state. Similarly, I_O is the inactivated state of the open state, which means that the conformation of I_O is established by a structural change from the open state. The channel protein conformations of the inactivated states I_C and I_O can be realized, respectively, only from the closed state C and open state O. That is, these state transitions are state-dependent. However, we assume here that the transition rates between C and I_C and between O and I_O are the same (both γ and δ as in Fig. 2.23b), and those between C and O and between I_C and I_O are the same (both α and β as in Fig. 2.23b). Then the channel dynamics can be represented both by the Markov and the HH-based. The Markov model of this channel is described as

$$\frac{dC}{dt} = \beta O + \delta I_C - (\alpha + \gamma)C, \tag{2.98}$$

$$\frac{dO}{dt} = \alpha C + \delta I_O - (\beta + \gamma)O, \tag{2.99}$$

$$\frac{dI_C}{dt} = \beta I_O + \gamma C - (\alpha + \delta)I_C, \tag{2.100}$$

$$\frac{dI_O}{dt} = \alpha I_C + \gamma O - (\beta + \delta)I_O. \tag{2.101}$$

For the corresponding HH-based gate model, we need to be patient with loosing some detailed information about the channel conformation. We hypothesize two gate variables, m and h, where the variable m represents the probability that the channel state is in either O or I_O, and the variable h represents the probability that the channel state is in either O or C. Then $(1-m)$ represents the probability that the channel state is in either C or I_C, and $(1-h)$ represents the probability that the channel state is in either I_O or I_C. If we are aware of the conformations used in the Markov model, this seems strange, but with the assumption above, this modeling with m and h will work, and the open probability of the channel is represented as mh with the ODEs as follows.

$$\frac{dm}{dt} = \alpha(1-m) - \beta m,$$

$$\frac{dh}{dt} = \delta(1-h) - \gamma h.$$

This HH-based formulation is possible because we have assumed that the two horizontal transitions are identical and the two vertical transitions are also identical. Without these particular assumptions, this model essentially involves state dependent transitions, and it cannot be described by the HH formulation.

State transitions for the last example are shown in Fig. 2.23c. This can be modeled only by the Markov scheme, not by the HH-based gating model, because the inactivated state I can be realized only from the open state O. The Markov model of this channel is described as

$$\begin{aligned}\frac{dC}{dt} &= \alpha C - \beta O,\\ \frac{dO}{dt} &= \alpha C + \delta I - (\beta+\gamma)O,\\ \frac{dI}{dt} &= \gamma O - \delta I.\end{aligned} \tag{2.102}$$

Mathematically speaking, (2.102) for example, can be respresented as

$$\frac{d}{dt}\begin{pmatrix} C \\ O \\ I \end{pmatrix} = \begin{pmatrix} \alpha & -\beta & 0 \\ \alpha & -(\beta+\gamma) & \delta \\ 0 & \gamma & -\delta \end{pmatrix}\begin{pmatrix} C \\ O \\ I \end{pmatrix} \tag{2.103}$$

If the elements of the matrix are constant in a simple case, dynamics of the equation can be analyzed based on the eigenvalues and eigenvectors of the matrix.

IDE Modeling: L-Type Calcium Channel: Search ModelDB by "Rudy" to Find Faber_Rudy_2007_Model.isml

$$I_{Ca(L)} = \bar{I}_{Ca} O, \tag{2.104}$$

$$\bar{I}_{Ca} = P_{Ca} z_{Ca}^2 \frac{V_m F^2}{RT} \cdot \frac{\gamma_{Cai}[Ca^{2+}]_{ss} \exp\left(\frac{z_{Ca} V_m F}{RT}\right) - \gamma_{Cao}[Ca^{2+}]_o}{\exp\left(\frac{z_{Ca} V_m F}{RT}\right) - 1} \tag{2.105}$$

where O is the probability that the state of L-Type calcium channel is in open state which is one of 14 states of a Markov-type channel model as described below. This is a model of L-type calcium channel used in the Faber–Rudy model that we examined its action potential above. The reader is asked to draw a transition diagram among those states as an exercise, and compare your diagram with the one shown in the paper by Faber et al. (2007). The Ca^{2+} current through this channel is proportional O as well as $\bar{I}_{Ca}$. The $\bar{I}_{Ca}$ is the ion channel current model based on the famous *Goldman–Hodgkin–Katz (GHK) equation*, which is another way to model membrane channel currents (see below).

$$
\begin{aligned}
\frac{dC_0}{dt} &= \beta_0 C_1 + \theta C_{0Ca} - (\alpha_0 + \delta) C_0, \\
\frac{dC_1}{dt} &= \alpha_0 C_0 + \beta_1 C_2 + \theta C_{1Ca} - (\alpha_1 + \beta_0 + \delta) C_1, \\
\frac{dC_2}{dt} &= \alpha_1 C_1 + \beta_2 C_3 + \theta C_{2Ca} - (\alpha_2 + \beta_1 + \delta) C_2, \\
\frac{dC_3}{dt} &= \alpha_2 C_2 + \beta_3 O + \omega_f I_{Vf} + \omega_s I_{Vs} \\
&\quad + \theta C_{3Ca} - (\alpha_3 + \beta_3 + \gamma_f + \gamma_s + \delta), \\
\frac{dO}{dt} &= \alpha_3 C_3 + \lambda_f I_{Vf} + \lambda_s I_{Vs} + \theta I_{Ca} - (\beta_3 + \phi_f + \phi_s + \delta) O, \\
\frac{dI_{Vf}}{dt} &= \gamma_f C_3 + \phi_f O + \omega_{sf} I_{Vs} + \theta I_{VfCa} - (\omega_f + \lambda_f + \omega_{fs} + \delta) I_{Vf}, \\
\frac{dI_{Vs}}{dt} &= \gamma_s C_3 + \phi_s + \omega_{fs} I_{Vf} + \theta I_{VsCa} - (\omega_s + \lambda_s + \omega_{sf} + \delta) I_{Vs}, \\
\frac{dC_{0Ca}}{dt} &= \beta_0 C_{1Ca} + \delta C_0 - (\alpha_0 + \theta) C_{0Ca}, \\
\frac{dC_{1Ca}}{dt} &= \alpha_0 C_{0Ca} + \beta_1 C_{2Ca} + \delta C_1 - (\alpha_1 + \beta_0 + \theta) C_{1Ca}, \\
\frac{dC_{2Ca}}{dt} &= \alpha_1 C_{1Ca} + \beta_2 C_{3Ca} + \delta C_2 - (\alpha_2 + \beta_1 + \theta) C_{2Ca}, \\
\frac{dC_{3Ca}}{dt} &= \alpha_2 C_{2Ca} + \beta_3 I_{Ca} + \omega_f I_{VfCa} + \omega_s I_{VsCa} \\
&\quad + \delta C_3 - (\alpha_3 + \beta_2 + \gamma_f + \gamma_s + \theta) C_{3Ca}, \\
\frac{dC_{Ca}}{dt} &= \alpha_3 C_{3Ca} + \lambda_f I_{VfCa} + \lambda_s I_{VsCa} + \delta O - (\beta_3 + \phi_f + \phi_s + \theta) I_{Ca},
\end{aligned}
$$

$$\frac{dI_{VfCa}}{dt} = \gamma_f C_{3Ca} + \phi_f I_{Ca} + \omega_{sf} I_{VsCa} + \delta I_{Vf} - (\omega_f + \lambda_f + \omega_{fs} + \theta) I_{VfCa},$$
$$\frac{dI_{VsCa}}{dt} = \gamma_s C_{3Ca} + \phi_s I_{Ca} + \omega_{fs} I_{VfCa} + \delta I_{Vs} - (\omega_s + \lambda_s + \omega_{sf} + \theta) I_{VsCa} \tag{2.106}$$

where most of the Greek letter coefficients are voltage-dependent, and δ is calcium concentration dependent. The reader is asked to simulate the dynamics of this L-type calcium channel by isolating the module representing the L-type calcium channel from the Faber–Rudy model that can be downloaded from the ModelDB. For the IDE operation to perform the module isolation, see the later chapter of this textbook.

Here let us briefly explore the GHK equation to understand how the model of the current $\bar{I}_{Ca}$ in (2.105) is derived. We should be back in the story for the Nernst potential, in which we used the Nernst–Planck equation (2.13). In our context here, we consider a specific part of the cellular membrane (T-tubules) which is faced to the sarcoplasmic reticulum (SR). See Fig. 2.21. The dominant population of L-type calcium channels are typically embedded in the T-tubules of the membrane. $[Ca^{2+}]_{ss}$ used for the model of $\bar{I}_{Ca}$ is the calcium concentration of the dyadic subspace, the small space between the T-tubule membrane and the SR surface, while $[Ca^{2+}]_o$ is the calcium concentration outside the cellular membrane. Then (2.13) in our context becomes

$$J = -D\left(\frac{dc}{dx} + \frac{z_{ca}F}{RT} c \frac{d\phi}{dx}\right) \tag{2.107}$$

where z_{ca} is the valence of the calcium ion, and J the flux of calcium ions across the membrane. The GHK equation uses so-called the *constant field approximation*, which is a simplification such that the electric field within the membrane (i.e., within the lipid bilayer) can be assumed to be a constant. That is, electric potential is linear function of x as follows.

$$\phi(x) = -Kx$$

where K is a constant, for which the electric field is

$$-\frac{d\phi(x)}{dx} = K \quad \text{(const.)}$$

Denoting electric potential outside ($x = x_o$) and inside ($x = x_i$) the membrane are ϕ_o and ϕ_i, respectively, we have $V_m = \phi_i - \phi_o$. By integrating the electric field from the outside to the inside the membrane as

$$-\int_{x_o}^{x_i} \frac{d\phi(x)}{dx} dx = \int_{x_o}^{x_i} K dx$$

and assuming the thickness of the membrane is $L = x_i - x_o$, we have $-V_m = KL$, and thus

$$K = -\frac{V_m}{L} \tag{2.108}$$

Using this, (2.107) can be rewritten as the ordinary differential equation with respect to the concentration $c(x)$ as follows.

$$\frac{dc(x)}{dx} = \frac{z_{ca}FV_m}{RTL}c(x) - \frac{J}{D}. \tag{2.109}$$

We integrate (2.109) by spatial coordinate x from x_i to x_o to obtain the flux J as a function of c_i, c_o, and V_m. To this end, (2.109) is rewritten as

$$\frac{dc(x)}{dx} = \frac{z_{ca}FV_m}{RTL}\left(c(x) - \frac{RTLJ}{z_{ca}FV_mD}\right)$$

The variable transform $y(x) = c(x) - RTLJ/(z_{ca}FV_mD)$ is performed to obtain the simpler representation of (2.109) with respect to y as

$$\frac{dy}{y} = \frac{z_{ca}FV_m}{RTL}dx. \tag{2.110}$$

Exercise 2.3. Show that

$$J = \frac{z_{ca}FV_mD}{RTL}\frac{\gamma_{Cai}[Ca^{2+}]_{ss}\exp\left(\frac{z_{ca}FV_m}{RT}\right) - \gamma_{Cao}[Ca^{2+}]_o}{\exp\left(\frac{z_{ca}FV_m}{RT}\right) - 1} \tag{2.111}$$

by integrating (2.110) from $y_i = c_i - RTLJ/(z_{ca}FV_mD)$ to $y_o = c_o - RTLJ/(z_{ca}FV_mD)$ for the left-hand-side and from x_i to x_o for the right-hand-side, and by using the facts that $x_o - x_i = -L$, and also c_i and c_o can be described by "effective" calcium concentrations inside and outside the membrane, namely, $c_i = \gamma_{Cai}[Ca^{2+}]_{ss}$ and $c_o = \gamma_{Cao}[Ca^{2+}]_o$ for the Faber–Rudy model. γ_{Cai} and γ_{Cao} are referred to as the activity coefficients and represent, respectively, how the calcium ions of the subspace (inside) and outside of the membrane are deviated from the thermodynamic ideal solutes.

The calcium current through the L-type calcium channel $\bar{I}_{Ca}$ when the channel is in the open state ($O = 1$) can then be obtained by multiplying $z_{ca}F$ and (2.111) and denoting D/L as P_{Ca}, leading to (2.105). The ion current modeled by the GHK equation looks relatively complicated and possesses nonlinear dependence on the membrane potential V_m, but both the GHK model and the HH-type linear voltage dependency with the Nernst potential can be derived from the same Planck equation. Thus the use of either the GHK or the Nernst potential is not a matter of degree of modeling refinement. Electrophysiologists choose one of them that can reproduce more satisfactory than the other. Usually, it might be more suitable to use the GHK model rather than the Nernst-potential-based Ohmic model when differences in ion concentrations between inside and outside the membrane are large, in which the

current-voltage relationship tends to be nonlinear. Note that the (2.105) is a combination of the GHK current equation and the 14-states Markov-type channel kinetics, which is rather refined and detailed model.

2.8 Variety of Complex Dynamics of Cellular Excitations

Temporal patterns observed in a sequence of action potentials generated by single cells can be complicated. We have seen such a case in the FHN (BVP) with external periodic pulsatile stimulations. In fact, single cells without any external temporally-structured stimulations can autonomously produce complicated patterns of excitation, for example rhythmic bursting excitation.

As such an example, let us consider a model of a pancreatic β cell that shows repetitive, complex, and oscillatory bursting action potentials. Bursting action potentials (spikes) with active (spiking) and silent (non-spiking) phases in the membrane potential of the β cell of the pancreatic islet are induced by glucose, during which insulin is released from the β cell. Insulin is a hormone responsible for the homeostatic mechanism of blood glucose level. It regulates the glucose metabolism by taking up glucose from the blood and by storing metabolites (glycogen) into the liver and muscle cells. In the process of insulin secretion from the β cells, increase of transported glucose into the β cell by a transporter protein (GLUT2) results in increase of ATP released from mitochondrion, which then induces closure of ATP sensitive K^+ channels on the plasma membrane, leading to membrane depolarization. This then triggers opening of voltage-dependent Ca^{2+} channels of the β cell, resulting in increase of intracellular calcium concentration together with Ca^{2+} release from endoplasmic reticulum (ER), which then triggers the secretion of the insulin. See Fig. 2.24. The duration of the active phase and spike frequency within each active phase are altered by the glucose concentration.

For generating bursting dynamics in β cells, as well as in other kinds of bursting cells, fast and slow dynamics interact each other. The fast dynamics are associated with generation of each action potential (spike), typically in a time scale of one or a few milliseconds. The slow dynamics are typically in a time scale of a hundred milliseconds, which are caused by different mechanisms, for example, slow oscillatory changes in cytoplasmic calcium concentration $[Ca^{2+}]_i$, slow dynamics in channel conductance, etc. This situation can be formulated in an abstract form as follows.

$$\frac{dx}{dt} = f(x, y) \tag{2.112}$$

$$\frac{dy}{dt} = \epsilon g(x, y) \tag{2.113}$$

where the system's state is represented by $(n + m)$-dimensional vector $(x, y)^T$ with n-dimensional vector x and m-dimensional vector y. $\epsilon \ll 1$ is a small positive constant. Since ϵ is small, dy/dt is small, meaning that the rate of change in

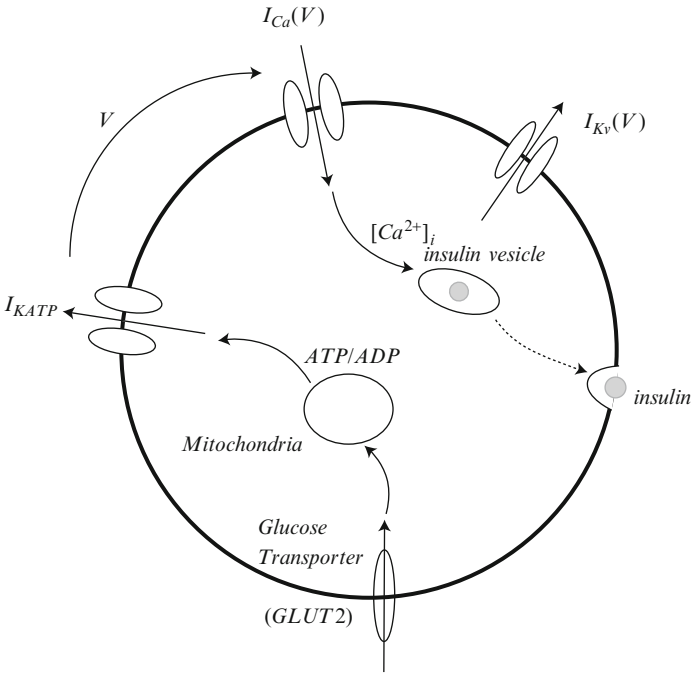


Fig. 2.24 Pancreatic β cell insulin secretion in response to glucose stimulation. Modified from Sherman and Bertram (2005)

the variable y is small and (2.113) represents the slow dynamics component of the whole model of $(x, y)^T$. Equation (2.112) for cellular membrane models exhibiting bursting dynamics describes action potential (spike) generation, that is, the fast dynamics component of the whole model. If we introduce a new time scale $t' = \epsilon t$ (or $t = t'/\epsilon$), the above set of equations can equivalently be rewritten as

$$\epsilon \frac{dx}{dt'} = f(x, y) \tag{2.114}$$

$$\frac{dy}{dt'} = g(x, y) \tag{2.115}$$

In the limit of $\epsilon \to 0$, we have

$$f(x, y) = 0$$

from (2.114), which may be solved formally as

$$x = x(y).$$

That is, x as a function of y. Substituting this into (2.113), we have

$$\frac{dy}{dt} = \epsilon g(x(y), y) \tag{2.116}$$

In many cellular membrane models exhibiting bursting dynamics, (2.116) of the y dynamics shows slow oscillation such as slow calcium oscillations. This slow oscillation may or may not be autonomous, but usually driven by the fast changes in x. For the fast spiking dynamics of x in (2.112), y does not change much. In the limit of $\epsilon \to 0$ in (2.113), y can be regarded as the constant parameter. The spiking dynamics of (2.112) may alter depending on the parameter value of y, either repetitive spiking behavior or non-spiking non-depolarized behavior. In non-limiting situation, y is not really constant, but changes slowly. Thus, for some range of y, the fast dynamics exhibit spiking corresponding to the active phase of the burst, and for the remaining range of y, they show no spikes corresponding to the silent phase of the burst. This is a story of so-called the *fast–slow analysis* of bursting. See Rinzel and Lee (1987), Bertram et al. (1995), Izhikevich (2006) for details. For this material, it is required to study bifurcation phenomena in nonlinear dynamical systems.

IDE Modeling: Bursting Oscillation in a Model Pancreatic β Cell: Search ModelDB by "Beta Cell" to Find Keizer_Smolen_1991.isml

$$C\frac{dV}{dt} = -I_{Ca} - I_{Kv} - I_{KATP} \tag{2.117}$$

where I_{Ca} is the calcium current, I_{Kv} the delayed rectifier potassium current, and I_{KATP} the ATP-sensitive potassium current. This pancreatic β-cell model is proposed by Keizer and Smolen (1991). Some details of three currents are as follows:

$$\frac{dJ}{dt} = -\frac{J - J^{\infty}(V)}{\tau_J(V)},$$

$$\frac{dn}{dt} = -\frac{n - n^{\infty}(V)}{\tau_n(V)},$$

$$I_{Ca} = \frac{g_{Ca}[Ca^{2+}]_o V}{[1 - \exp\left(\frac{2FV}{RT}\right)]},$$

$$I_{KATP} = G_{KATP}(V - V_K),$$

$$g_{Ca} = \bar{g}_{Ca}\left(PO_f \cdot X_f + m_s^{\infty}(V)J(1 - X_f)\right),$$

where J is the slow voltage inactivation of the calcium current, n the gating variable for the delayed rectifier potassium current. I_{Ca} is basically modeled by the Goldman–Hodgkin–Katz (GHK) formulation. The first term of the channel conductance g_{Ca} represents the fast spiking component, which is determined by PO_f dynamics (ODE is not shown), the fraction of open calcium channel of its fast dynamics modeled by a Markov-type state transition. X_f is a static constant representing a fraction of the maximum conductance for the fast component. The second

term of g_{Ca} represents the slow dynamics of the calcium channel responsible for the remaining fraction of the calcium conductance $(1 - X_f)$, and it is regulated by the slow inactivation gating dynamics of J. This slow component of the calcium current generates the slow oscillation in the membrane potential on which the fast spiking dynamics is superposed in a nonlinear manner, leading to the bursting dynamics of the model. Figure 2.25-upper shows a snapshot of the IDE with this Keizer and Smole model. In the lower panel, bursting dynamics of the membrane potential with the slow gating dynamics of J are simulated by the *insilico*IDE. The reader is asked to reproduce this with your downloaded model.

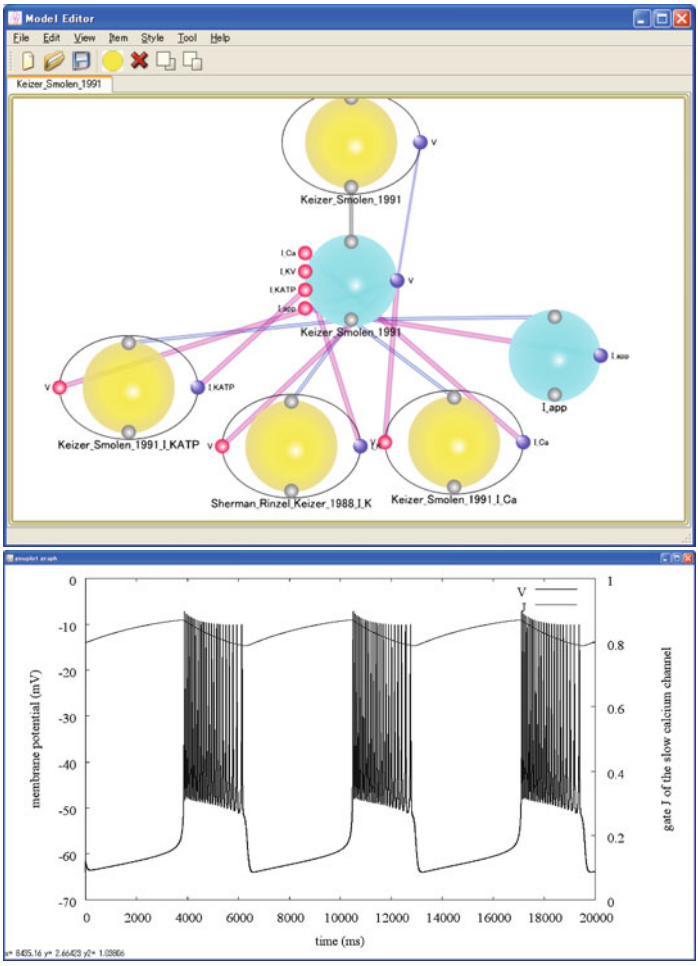


Fig. 2.25 *Upper*: A snapshot of *insilico*IDE for the Keizer–Smolen model of a pancreatic β cell. *Lower:* Bursting action potential of the model. *Thick-solid curve* represents the membrane potential V, the *thin solid* the gate variable J of the slow component of the calcium channel in the right vertical axis scale

2.9 Cellular Calcium Dynamics

Dynamics of intracellular Ca^{2+} are often under tight control by various mechanisms. Ca^{2+} in the dyadic subspace of cardiac cell can be crucial for contraction of myocyte. We have examined the calcium dynamics in the dyadic subspace using the Faber–Rudy (FR) model and its L-type calcium channel modeling, where intracellular Ca^{2+} regulates the amount of Ca^{2+} influx across the sarcolemma through Ca^{2+}-dependent inactivation of the L-type calcium channel. This mechanism is important in the regulation of cardiac *excitation-contraction coupling*. In the FR model, though it is one of the most detailed and complex electrophysiological models of cardiac cellular excitation and calcium dynamics, intracellular calcium dynamics are just modeled by a simple set of ordinary differential equations. See (2.95), for example. If we need to focus the intracellular calcium dynamics more in detail, it will be required to consider spatial dimension and geometry of the intracellular space.

One way to take into account spatial dimension and cytoplasmic geometry is to consider diffusion of calcium ions within the intracellular space. As we learned in (2.10), Fick's law is used here for three-dimensional space with its coordinate $x = (x_1, x_2, x_3)$.

$$J(x,t) = \begin{pmatrix} J_1(x,t) \\ J_2(x,t) \\ J_3(x,t) \end{pmatrix} = -D\nabla[Ca^{2+}](x,t) \equiv -D \begin{pmatrix} \dfrac{\partial[Ca^{2+}](x,t)}{\partial x_1} \\ \dfrac{\partial[Ca^{2+}](x,t)}{\partial x_2} \\ \dfrac{\partial[Ca^{2+}](x,t)}{\partial x_3} \end{pmatrix} \tag{2.118}$$

where $[Ca^{2+}](x,t)$, which is a function of time t and space x, represents the calcium ion concentration at the intracellular space at time t and at the position x. The first, second, and the third component of the J_c represent the flux, the amount of ions that flow through a unit area within a unit time interval in the x_1, x_2, and x_3 direction, respectively. Thus, a change in the amount of calcium ions within in a small cubic of volume $\Delta x_1 \Delta x_2 \Delta x_3$ within a small time interval Δt can be represented as

$$\begin{aligned} &\left([Ca^{2+}](x,t+\Delta t) - [Ca^{2+}](x,t)\right) \Delta x_1 \Delta x_2 \Delta x_3 = \\ &\quad [J_1(x_1,x_2,x_3) - J_1(x_1+\Delta x_1,x_2,x_3)]\,\Delta x_2 \Delta x_3 \\ &\quad [J_2(x_1,x_2,x_3) - J_2(x_1,x_2+\Delta x_2,x_3)]\,\Delta x_3 \Delta x_1 \\ &\quad [J_3(x_1,x_2,x_3) - J_3(x_1,x_2,x_3+\Delta x_3)]\,\Delta x_2 \Delta x_3 \end{aligned} \tag{2.119}$$

The first term of the right hand side is the amount of ions flowing in the x_1 direction into the volume from the square with its area $\Delta x_2 \Delta x_3$ and flowing out the volume from the square with its area $\Delta x_2 \Delta x_3$. See Fig. 2.26. The second and third terms are defined similarly for the x_2 and x_3 directions, resulting in this equation of balance,

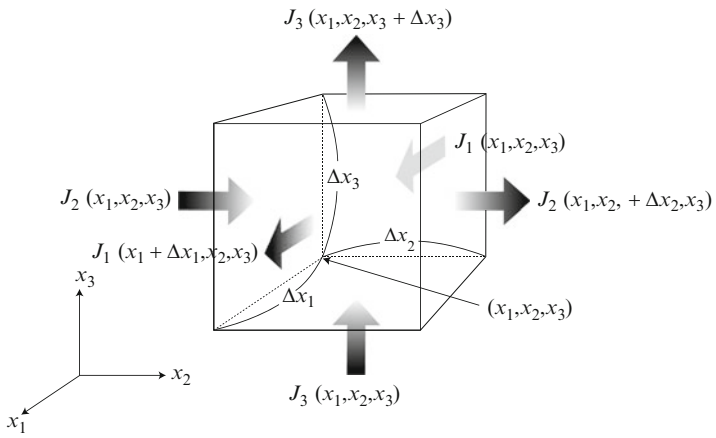


Fig. 2.26 Diffusion of calcium ions in a three dimensional space

referred to as the *equation of continuity*. By taking a limit $\Delta x_i \to 0$ for $i = 1, 2,$ and 3, we have the following equation

$$\begin{aligned}\frac{\partial [Ca^{2+}](x,t)}{\partial t} &= D\nabla^2[Ca^{2+}](x,t) \\ &\equiv D\left(\frac{\partial^2[Ca^{2+}](x,t)}{\partial x_1^2} + \frac{\partial^2[Ca^{2+}](x,t)}{\partial x_2^2} + \frac{\partial^2[Ca^{2+}](x,t)}{\partial x_3^2}\right)\end{aligned} \tag{2.120}$$

referred to as the *diffusion equation*.

Exercise 2.4. Derive (2.120) from (2.119) using (2.118).

If the diffusion of the calcium takes place in a space with no boundary (infinitely large free space), we can assume that $[\mathrm{Ca}^{2+}](x,t)$ goes to zero smoothly as $|x| \to \infty$. Thus, (2.120) will be solved with boundary conditions

$$\frac{\partial [Ca^{2+}]}{\partial x_i}(\pm\infty, t) = 0$$

for $i = 1, 2,$ and 3. If the diffusion takes place in a space limited by barriers such as membrane and the surface of cellular organelle, (2.120) should be solved with boundary conditions defined for the surface of the barriers. The calcium ions flowed through the calcium channels into the dyadic subspace of the cardiac myocite diffuse within the dyadic space. In this case, the boundaries are the plasma membrane and the SR surface.

The dyadic space where the calcium ions diffuse are full of proteins such as calcium buffers and calcium binding proteins (Tanskanen et al. 2007). A major calcium binding protein is calmodulin (CaM). It forms a CaM–Ca^{2+} complex when Ca^{2+}

binds to the CaM. CaM and CaM–Ca^{2+} complex also bind to a number of different proteins, by which they regulate various cellular functions. In this way, Ca^{2+} ions diffuse within the dyadic space with interacting with those proteins. Let us consider a diffusion of calcium ions in the presence of calcium buffer molecules B that bind and unbind with Ca^{2+} according to the following chemical reaction.

$$Ca^{2+} + B \underset{k_-}{\overset{k^+}{\rightleftharpoons}} CaB \tag{2.121}$$

Using the *law of mass action*, changes in the calcium concentration caused by this reaction is described as

$$\frac{d[Ca^{2+}]}{dt} = -k_+[Ca^{2+}][B] + k_-[CaB] \tag{2.122}$$

where k_+ and k_- are the reaction rate constants, respectively, for the association (binding) and dissociation (unbinding) of Ca^{2+} with CaM. The first term of the right hand side of (2.122), $[Ca^{2+}][B]$, may be proportional to the number of distinct combinations of the free calciums and the Ca^{2+}-free buffers, and occurrence probability of collisions between free Ca^{2+} and Ca^{2+}-free B may be proportional to this number. If this number of combinations is large, the reaction proceeds rightward frequently to produce CaB complex and the number of free calcium (thus $[Ca^{2+}]$) decreases. Similarly, for the second term, the leftward reaction occurs more frequently as the $[CaB]$ increases, contributing to the increase of $[Ca^{2+}]$. Changes in $[B]$ and $[CaB]$ can similarly be formulated as

$$\frac{d[B]}{dt} = -k_+[Ca^{2+}][B] + k_-[CaB],$$

$$\frac{d[CaB]}{dt} = k_+[Ca^{2+}][B] - k_-[CaB].$$

In the dyadic space, this type of chemical reactions occur in a position x-dependent manner. Thus, with the diffusion dynamics, the spatio-temporal dynamics of the calcium concentration can be described as

$$\frac{\partial[Ca^{2+}]}{\partial t} = D\nabla^2[Ca^{2+}] - k_+[Ca^{2+}][B] + k_-[CaB] \tag{2.123}$$

$$\frac{\partial[B]}{\partial t} = D_B\nabla^2[B] - k_+[Ca^{2+}][B] + k_-[CaB] \tag{2.124}$$

$$\frac{\partial[CaB]}{\partial t} = D_{CaB}\nabla^2[CaB] + k_+[Ca^{2+}][B] - k_-[CaB] \tag{2.125}$$

where D_B and D_{CaB} are the diffusion coefficients of B and CaB, respectively, and they are smaller than D because the buffers are large molecules. For theoretical analyses of this set of reaction diffusion equations, see Ait-Haddou et al. (2010) for

example, in which it is shown that the "effective" calcium diffusion can be slow in comparison with that without the buffers if the buffers are present in excess. The effective calcium diffusion coefficient D_{eff} may be formulated as

$$D_{eff} = \frac{D + \kappa D_B}{1 + \kappa} \tag{2.126}$$

where

$$\kappa = \frac{K_d [B]_T}{(K_d + [Ca^{2+}]_\infty)^2}$$

with $K_d = k^+/k_-$, the dissociation constant, $[B]_T = [B] + [CaB]$, the total buffer concentration, which is assumed to be a constant and spatially uniform here. $[Ca]_\infty$ is the free calcium concentration at the equilibrium state. At high buffer concentrations, i.e., at high concentration of $[B]_T$, there left only small amount of free calcium. Thus, if K_d is relatively small, $\kappa \gg 1$, leading to small D_{eff}. This suggests that seemingly simple diffusion of intracellular calcium could be affected by reactions between the calcium and buffer proteins.

2.10 Bridging Between Different Levels of Modeling: A Preliminary Example

Here we consider a simple example that can bridge between two different levels of modeling for intracellular calcium dynamics. In one level, the calcium dynamics within the dyadic subspace of a cardiac myocyte are modeled by an ordinary differential equation referred to as the ODE model or the cellular level model constructed for a whole cell electrophysiology of cardiac cellular excitation. To this end, we use the Faber–Rudy (FR) model again. In the other level, modeling focuses details of the calcium dynamics within the dyadic subspace, in which a model of the calcium dynamics with a geometrical model of the dyadic subspace is constructed using a *Multi-Agent-Simulation* model (MAS) or *Monte Carlo simulation* methodology, referred to as the MAS model or the subcellular level model.

Dynamic changes in the calcium concentration, $[Ca^{2+}]_{ss}$, within the dyadic subspace are of importance because they involve key processes connecting electrophysiology of each cardiac myocyte and mechanical contraction of the cell. For making the regulations of $[Ca^{2+}]_{ss}$ fine and tight, for example, the L-type calcium channel is both voltage and $[Ca^{2+}]_{ss}$ dependent. Particularly, it is inactivated when $[Ca^{2+}]_{ss}$ increases. The L-type calcium channels on the plasma membrane are located in close vicinity to the corresponding SR surface (see Fig. 2.21) on which the ryanodine receptors are arrayed and they trigger the calcium release necessary for muscle contractions in response to increase of $[Ca^{2+}]_{ss}$ by the calcium influx from the L-type calcium channels. Recent studies show that localized and time-dependent calcium concentration within the dyadic subspace, as well as the global-averaged

calcium concentration of the subspace, are engaged to the regulation of kinetics of the L-type calcium channel (Tadross et al. 2008).

The ODE (cellular level) model of subspace calcium dynamics in the FR model are described, as in (2.94), by

$$\frac{d[Ca^{2+}]_{ss}}{dt} = -\beta_{ss}\left((I_{Ca(L)} - 2I_{NaCa,ss})\frac{A_{cap}}{V_{ss}z_{ca}F} - I_{rel}\frac{V_{JSR}}{V_{ss}} + I_{diff}\right), \quad (2.127)$$

where $I_{Ca(L)}$, $I_{NaCa,ss}$, I_{rel} modeled by Markov type receptor kinetics (equations are not shown), and I_{diff} represent, respectively, the currents of the L-type calcium channel with the Markov model as in (2.104), the Na^+–Ca^{2+} exchanger in the subspace, the calcium release from the SR into the dyadic subspace inducing a rapid and large increase of $[Ca^{2+}]_{ss}$ referred to as the calcium induced calcium release (CICR), and the calcium diffusion between the dyadic subspace and the cytoplasmic space. I_{diff} is modeled as

$$I_{diff} = \frac{[Ca^{2+}]_{ss} - [Ca^{2+}]_i}{\tau_{diff}} \quad (2.128)$$

where $[Ca^{2+}]_i$ is the cytoplasmic calcium concentration as in (2.95). There are many subspaces in the cytoplasmic space, each of which is a narrow microspace between the plasma membrane and each of many SR surfaces. In the FR model, however, they are lumped together as a single space (a compartment) whose surface area A_{cap} and volume V_{ss} are set to be equal to those of the sum of all subspaces. The calcium diffusion considered in (2.128) is thus the calcium flow between two compartmental spaces, namely, the single compartment as the dyadic subspace and the cytoplasmic space. The Ca^{2+} flow is determined so that it is proportional to the concentration difference between those two spaces. The constant τ_{diff} determines the speed of this diffusion. In the FR model, the constant $\tau_{diff} = 0.1$ ms is utilized.

The solid curve in Fig. 2.27 shows dynamics of the calcium concentration in the dyadic subspace during a voltage clamp condition obtained by the ODE model. In this simulation, the cytoplasmic calcium concentration is fixed at $[Ca^{2+}]_i = 6.72 \times 10^{-5}$ mM. In response to the voltage clamp step applied at $t = 0$, the L-type calcium channel begins to open, and its calcium influx increases rapidly the $[Ca^{2+}]_{ss}$, which induce the calcium release current I_{rel} from the SR, leading to the CICR and the peak calcium concentration $[Ca^{2+}]_{ss}$ about 0.014 mM. The increase of $[Ca^{2+}]_{ss}$ inactivates the L-type calcium channel and the calcium ions in the dyadic subspace diffuse out into the cytoplasmic subspace, and thus the $[Ca^{2+}]_{ss}$ decreases.

The MAS (subcellular level) model concentrates the calcium diffusion within a single dyadic subspace. The single dyadic subspace is modeled as a microspace between the plasma membrane with its area 200 × 200 nm and the corresponding SR membrane with the same area. The distance between the plasma membrane and the SR surface is set to 50 nm. On the SR membrane, cubic-like-shaped ryanodine receptors are configurated. See Fig. 2.28 for overall model geometry. On the plasma

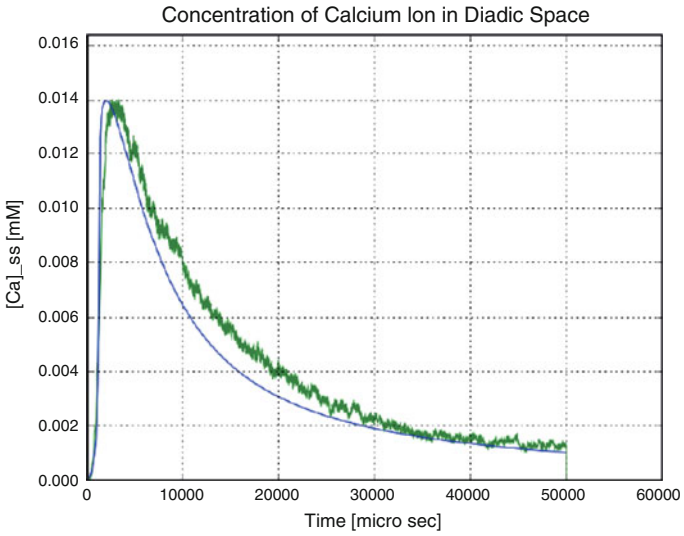


Fig. 2.27 Calcium concentration in the dyadic space obtained by MAS and ODE

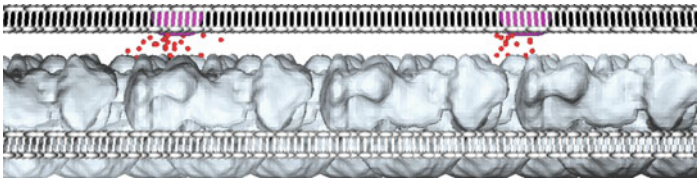


Fig. 2.28 Calcium influx through L-type calcium channels and diffusion within a cellular dyadic space

membrane, four L-type calcium channels are arrayed from which individual Ca^{2+} ion particles are flowed into the subspace if the corresponding L-type channel is in its open state. Each of the L-type calcium channels is modeled using the one used in the FR model, but its kinetics is simulated using a Monte Carlo method implemented as an agent of MAS model. That is, a sample sequence of the state transitions of the Markov model described by (2.106) is realized stochastically using a sequence of pseudo random-numbers without solving the ODEs. For example, let us illustrate this for generating a sample random sequence corresponding to the first ODE of (2.106),

$$\frac{dC_0}{dt} = \beta_0 C_1 + \theta C_{0Ca} - (\alpha_0 + \delta)C_0.$$

This ODE describes changes in the probability that the state of the L-type calcium channel is at C_0, one of the closed states. The state C_0 will move to either C_1 with the rate constant α_0 or to C_{0Ca} with the rate constant δ. The state C_0 is visited

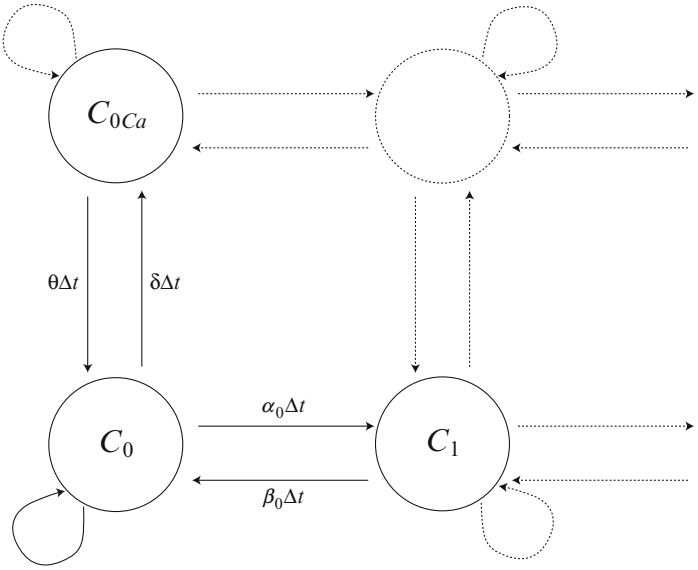


Fig. 2.29 Markov chain representation of a part of the L-type calcium channel

by the transitions from C_1 with the rate constant β_0 and from C_{0Ca} with the rate constant θ. In terms of the MAS or Monte Carlo simulation, this process is modeled by the following Markov chain. See Fig. 2.29. Let us assume that the state is at C_0 at time t, and consider how it moves to other states or it stays at the same state C_0 after the time elapse of Δt. Possible outcomes at $t + \Delta t$ and the corresponding probabilities are as follows.

- Move to the state C_1 with the probability $\alpha_0 \Delta t$
- Move to the state C_{0Ca} with the probability $\delta \Delta t$
- Keep staying at the state C_0 with the probability $1 - \alpha_0 \Delta t - \delta \Delta t$

The state located initially at C_0 may reach the open state O by continuing such stochastics transitions during a single simulation of a given duration. In Fig. 2.27, the time span of a single simulation was set to 50,000 μs. $\Delta t = 1$ ns was used. If the channel state of a L-type calcium channel is in the open state O at a time instant t, a single Ca^{2+} ion particle is created at the position of the pore of the L-type calcium channel in the time interval Δt with the probability 1.92×10^{-2} which corresponds to a single channel current of 6.15×10^{-3} pA. The state transition of each ryanodine receptor is simulated similarly, and if its state is at the open state, a single Ca^{2+} particle is created in Δt at the position of the pore of the ryanodine receptor with the probability 0.8×10^{-2} to simulate the calcium induced calcium release. Some part of transition probabilities in both the L-type calcium channel and the ryanodine receptor are $[Ca^{2+}]_{ss}$-dependent, representing the calcium dependent inactivation for the L-type channels and the calcium induced calcium release from the SR for the ryanodine receptors.

Individual calcium ion particles flowed into the dyadic subspace from the L-type calcium channels and the ryanodine receptors diffuse within the space with the geometry shown in Fig. 2.28. In the MAS-subcellular model, the diffusion of each calcium ion particle is modeled by a simple unbiased Brownian motion. To this end, the dyadic space is discretized into a number of cubics with each side length of Δx. Each calcium ion particle is located at one of their apices at an instant t, and it moves stochastically to one of its six nearest neighbor apices with the identical probabilities, or stay at the same position, for every small time step $\Delta t_D = 0.1$ ns, which is smaller than $\Delta t = 1$ ns used for the state update of the L-type calcium channels and the ryanodine receptors. If a calcium ion particle is going to hit the wall of the dyadic space, i.e., the plasma membrane, the SR surface, or the surface of the ryanodine receptors, by the next time step movement, it is assumed that the ion particle stays at the same position.

For a given time step Δt_D (in this case 0.1 ns), the diffusion speed of each ion particle is determined by the one step length of movement Δx. A large step length corresponds to a large diffusion coefficient D_{Ca} in the diffusion equation. As we used in (2.12), the diffusion coefficient of a calcium ion is determined as

$$D_{Ca} = \frac{u_{Ca} RT}{|z_{Ca}| F}. \tag{2.129}$$

The diffusion coefficient of the calcium within the pure water is then calculated to be $1.58 \times 10^{-12}\,\mathrm{m}^2/\mathrm{ms}$. However, this value may not be appropriate in our simulation, because there are many calcium binding proteins within the dyadic space which may slow the effective calcium diffusion down as we discussed above. Let us denote the effective diffusion coefficient of the calcium ion particle within the dyadic space $\bar{D}_{Ca}$. Then, as we will see later in (3.18), the diffusion in a single direction from a point calcium source may time-evolve as

$$\exp\left(-\frac{x^2}{2\sigma^2 t}\right),$$

as the function of time of diffusion t, where

$$\sigma = \sqrt{2\bar{D}_{Ca} t}.$$

Therefore, for the small time step Δt_D, the ion particle may move in average about

$$\Delta x \sim \sqrt{2\bar{D}_{Ca} \Delta t_D} \tag{2.130}$$

The noisy curve shown in Fig. 2.27 represents dynamic change in the ensemble averaged $[Ca^{2+}]_{ss}$ within the single dyadic space of the MAS model from 400 sample paths, which show a good coincidence with the solid curve obtained from the ODE cellular level simulation on the FR model. In order to have this coincidence between the subcellular-level MAS model and the cellular-level ODE model,

the appropriate one step movement Δx that gives the coincidence was obtained in a trial and error approach. In this example, we got $\Delta x = 2.5\,\text{nm}$. From (2.130), the corresponding effective diffusion coefficient of the calcium ion is obtained as $\bar{D}_{Ca} = 4.91 \times 10^{-14}\,\text{m}^2/\text{ms}$, which is about 100 times smaller than the calcium diffusion coefficient in the pure water D_{Ca}.

This example gives a rough idea of how different levels (scales) of modeling are inter-related with each other. Since it may not be an easy task to obtain the diffusion coefficient of the calcium within the nanoscale dyadic space, but it could be crucial to understand how the calcium diffusion in the dyadic space is controlled for the excitation-contraction coupling, the approach taken in this example could be beneficial. MAS modeling, though it is computationally time consuming, can provide relatively easy ways to make the modeling more in detail, such as introducing calcium binding proteins in the dyadic space and taking the effect of electric field on the ion movement into account. Simulated data obtained by such mechanism-based detailed modeling should be compared with data obtained by one scale larger ODE modeling as well as by experimental data, leading to deeper understanding of how physiological functions emerge at multiple scales of time and space.

http://www.springer.com/978-4-431-53879-0

Harnessing Biological Complexity
An Introduction to Computational Physiology
Nomura, T.; Asai, Y.
2011, X, 190 p., Softcover
ISBN: 978-4-431-53879-0